Results in Engineering 25 (2025) 104402

Contents lists available at ScienceDirect

Results in Engineering

journal homepage: www.sciencedirect.com/journal/results-in-engineering

A comparative study of AVC-PDM and AVC-PWM based cyclo-inverter fed induction heating systems

S. Jaanaa Rubavathy [a,*], Sivapriya J [b], B. Durai Babu [c], K. Sasikala [d], S Gomathi [a]

[a] Department of Electrical and Electronics Engineering, Saveetha School of Engineering, SIMATS, Saveetha University, Chennai. 602105, Tamil Nadu, India
[b] Department of Chemistry, St. Joseph's Institute of Technology, Chennai 119, India
[c] Engineering Department, University of technology and applied sciences, Ibra, India
[d] Vels Institute of Science, Technology & Advanced Studies, Pallavaram, Chennai, Tamil Nadu, India

ARTICLE INFO

Keywords:
Asymmetrical voltage cancellation control
Pulse density modulation
Pulse width modulation
Cyclo-inverter
Induction heating
Energy
Efficiency

ABSTRACT

Wide spread advantages of high frequency techniques finds many applications in various fields. The latest contributions addressees' uniqueness and efficient requirements in the field of medical equipments, industrial and domestic heating, research areas etc. The primary purpose of this research is to offer extensive output power control in a Cyclo-inverter fed Induction Heating (IH) system by means of two different control techniques such as Asymmetrical Voltage Cancellation with Pulse Density Modulation (AVC-PDM) and Asymmetrical Voltage Cancellation with Pulse Width Modulation (AVC-PWM) technique. Fourier analysis of output voltage is conducted to assess the effectiveness of the suggested technique in addition to conventional one. To improve the dynamic response of resonant based Induction Heating (IH) system for power control, controllers are introduced in the feedback loop. In this work, Cyclo-inverter with Fuzzy Logic controller (FLC) is used so as to improve the transient behavior of the system. Moreover, a comparison of the Cyclo-inverter system is conducted and simulated using MATLAB/SIMULINK. The control logic is implemented on a Spartan 3E FPGA to validate the results.

1. Introduction

Induction heating is a method of heating that does not involve direct contact, which is utilized to attribute, solidify or create laxer metals or other conductive materials. As far as the induction heating is concerned, the literature on the subject is growing. Over the years a large number of induction heating applications are proposed by research scholars. A MOSFET switch-based series resonant inverter was suggested to improve the cooling system and power conversion efficiency in [1]. Control strategies such as Constant frequency (PWM, PDM), Phase shift control, Phase angle control and Power Frequency Modulation (PFM) were also given in [2–4] in order to regulate the output power. The most basic resonant inverter employed for IH purposes is the half-bridge series resonant inverter [5], which employs irregular driving patterns for controlling the output power.

Numerous topologies are utilized for induction heating purposes. Different topologies are used for induction heating applications. Multi-output (MO) full-bridge inverter setups have been investigated for regulating the power across load terminals via AVC or Asymmetrical PWM in [6] and [7]. [8] presents a performance evaluation of a MO cyclo-inverter powered IH system, focusing on various control methods for power management.

The efficiency of induction heating loads relies on both the power converter's efficiency and the induction heating load. This efficiency was enhanced by the quantitative evaluation of induction efficiency in [9], demonstrating that efficiencies greater than 95 % can be achieved with an appropriately designed inductor system. To reduce the number of components and further improve efficiency, a high-frequency AC-AC converter is proposed in [10].

New IH power supply system for forging applications which have good PF, increased efficiency, high power output and good performance characteristics is given in [11]. However the usual power supplies have reduced efficiency with low power factor. And [12], suggested a dual-frequency IH power supply circuit utilizing LLC load resonance technology. It utilizes a time-sharing control strategy by managing the on-off switching tube in the medium HF range, resulting in low cost and miniaturization of the IH power supply. The design [13] features two sets of half-bridge series resonant converters (HBSRI) operating at different resonant frequencies sharing a capacitor. These converters operate under the ADC modulation scheme for smooth functioning.

* Corresponding author.
E-mail address: jaanaarubavathys.sse@saveetha.com (S.J. Rubavathy).

https://doi.org/10.1016/j.rineng.2025.104402
Received 21 November 2024; Received in revised form 23 January 2025; Accepted 17 February 2025
Available online 19 February 2025

Unlike traditional topologies, the proposed design eliminates the need for a DC stage, connecting directly to the source of energy to generate a high-frequency (HF) AC output. This direct connection reduces the number of converter components compared to conventional designs, leading to decreased voltage drop, lower power losses, reduced costs, and enhanced efficiency. [14] Suggested a comprehensive induction heating system designed to efficiently heat both uniformly convex-bottom woks and pots with flat bottoms on a flat stovetop [16]. Pulse generation of the converter is strategically enhanced through the integration of AVC (Amplitude-Variable Control) and PDM (Pulse-Density Modulation) methods. built-in dead band in the AVC method facilitates soft switching, minimizing switching losses, whereas PDM increases the power control range without changing the switching frequency [17]. By utilizing soft switching, it minimizes switching losses and improves efficiency at low power levels, allowing for smooth power control through this modulation technique [18]. The IH system utilizes a half-bridge (HB) resonant converter, controlled through zero-voltage switching (ZVS). The multi-tapping winding helps transfer heat effectively by dividing the induction coils to match the vessel's size [19]. It provides perspectives on the future of induction heating uses, emphasizing the integration of semiconductor materials with a wide band-gap power, MO configurations, and variable-frequency control systems by means of reduced losses, as well as filters intended to raise pf at a source-side [20]. The synthesized converter acts as a multi-output extension of full-bridge technology, allowing independent and concurrent regulation of outputs at their rated power. This method reduces the number of components in contrast to single-output converter solutions and enhances the efficiency of electronic component utilization. The paper [21] reviews PWM techniques for harmonic suppression in power converters for renewable energy systems. It compares methods like Sinusoidal PWM and SVPWM, highlighting their advantages, limitations, and future prospects [22]. The paper focuses on the key features of converter topologies used in domestic and industrial heating applications. It evaluates performance based on factors like power conversion stages, efficiency, and future trends such as wide band-gap semiconductors and improved filter designs [23]. IH system based on this new concept offers several advantages over traditional induction heating systems and holds significant potential for commercial applications [24]. This study presents innovative converter and control models to enhance the performance, voltage gain, and power quality of a PV-EV system. The proposed Skill Optimized Power Tracker (SOPT) and Elman Network-based Fire Hawk Controller (IEFC) improve energy output, motor performance, and overall system efficiency [25]. The half-bridge series resonant inverter designed for induction heating (IH) applications operates in two distinct modes to optimize efficiency across a wide power range. At higher power levels, frequency control is employed, while pulse width modulation (PWM) is utilized at lower power levels. This dual-mode approach minimizes losses and improves the converter's overall efficiency throughout its entire operating range. The study in [26] analyzes coupled induction heating and solar energy for faster and efficient heating of cylindrical workpieces, It highlights potential applications in industrial heat treatments like annealing and quenching with reduced time and energy. This study [27] examines using induction furnace slag (IFS) as a substitute for brick or recycled brick aggregates to improve the strength and durability of concrete. Results demonstrate that incorporating IFS significantly improves concrete performance, addressing limitations like high water absorption and low strength in brick aggregate concrete. [28] examines the mechanical performance and fatigue crack growth (FCG) resistance of AISI 4140 steel under single- and multi-austempering heat treatments, emphasizing the superior properties of multi-austempered steel at 362 °C. The optimized bainitic structure, featuring larger martensitic-austenite islands and thicker retained austenite, improves tensile strength and maximizes FCG resistance.

The Proposed model is based on comparative analysis AVC-PDM & AVC-PWM based cyclo-inverter fed induction heating system for power control. This paper identifies the appropriate topology and control technique for output power regulation. The structure of the paper is as follows: Sections II and III detail the proposed Cyclo-inverter topology, along with simulation results for AVC-PDM and AVC-PWM. Section IV offers a Fourier analysis of the inverter output, while Sections V and VI compare the control techniques, analyze the transient response, and evaluate power factor improvement. Section VII focuses on the hardware implementation of the proposed system. Lastly, Section VIII concludes the study.

2. Proposed cyclo-inverter topology

A two-output Cyclo-inverter fed IH system is used for output power control using Constant Frequency operation. Two inductive loads used must have the characteristics of independent control over its rated output power simultaneously with constant frequency operation. It is fundamentally a power conversion circuit that transforms LFAC and HFAC at very high frequencies.

High-frequency Cyclo-inverter is an adaptation of the full-bridge series resonant inverter intended for applications in IH. But it eliminates the use of electrolytic capacitor in DC link between the rectifier and inverter modules. The functioning of the Cyclo-inverter configuration is quite comparable to that of the full bridge Series Resonant Inverter (FBSRI) topology. [15] but instead of supplying pure DC input it uses rectified (Pulsating) DC as input to the inverter.

The multi-output CI-IHS is given in Fig. 1. It consists of an uncontrolled rectifier which converts the AC mains voltage (V_{in}) of 50 cycles per second into its equivalent DC. This pulsating DC is now applied to the Cyclo-inverter. The resonant state is attained by using a resonant capacitor. (C_1 and C_2). The six MOSFET switches Q_1 to Q_6 are given with protection diodes, which are connected sequentially. For obtaining the power from first load, leg one switches (Q_1 and Q_2) along with common leg switches (Q_5 and Q_6) are operated. Similarly for a second load, leg two switches (Q_3 and Q_4) along with common leg switches (Q_5 and Q_6) are operated. The high-frequency current produced by this inverter is supplied to the working coil, which can create the required heating by inducing eddy currents. Resonant condition is achieved by using resonant capacitors (C_1&C_2) linked with the equivalent resistance and inductance of load arrangement. Switching losses in all the MOSFET devices are reduced by using Zero Voltage Switching (ZVS) for each MOSFET.

3. Simulation results of open loop system

The inverter generates a HF current that is devlivered to the working coil, which can create the required heating by inducing eddy currents in the workpiece. The Cyclo-inverter architecture is modeled and simulated in MATLAB-Simulink to validate the dual-output system for IH. The simulation design parameters are listed in Table 1.

3.1. Open loop system with AVC-PDM control

The AVC-PDM (Asymmetrical Voltage Cancellation - Pulse Density Modulation) control technique employed for induction heating applications integrates two strategies: Asymmetrical Voltage Cancellation (AVC) and Pulse Density Modulation (PDM). AVC works by adjusting the phase and magnitude of the voltage applied to the system, effectively canceling unwanted voltage components to enhance the power transfer efficiency and reduce harmonic distortion. PDM, on the other hand, regulates the power delivered to the induction heater by controlling the pulse density in response to the required heating demand. This combination allows for precise control of the power supplied to the induction heating system, ensuring efficient energy usage, stable temperature control, and improved system performance while minimizing thermal stress and power losses.

The required PDM switching pulses is generated by logically

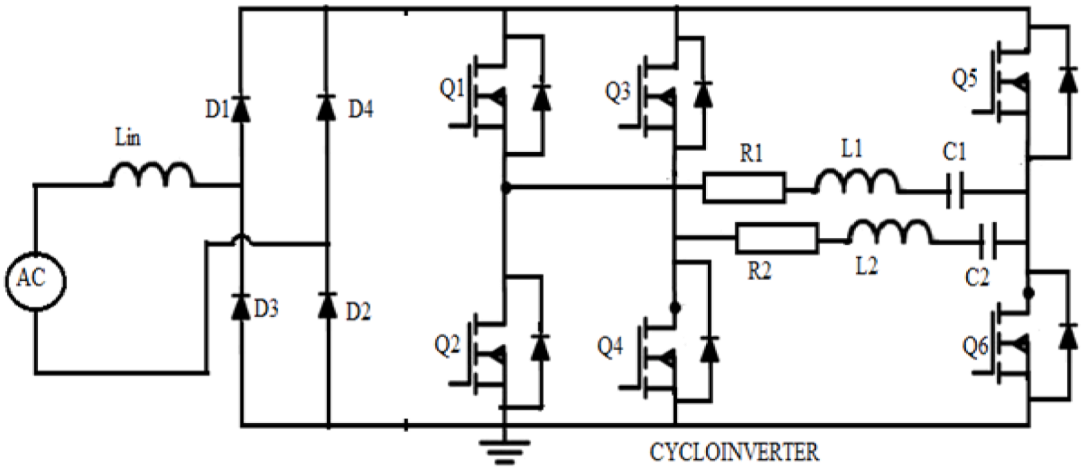

Fig. 1. Multi-output Cyclo-inverter fed IH system.

Table 1
Simulation parameters of Cyclo-inverter.

S. No.	Parameters	Symbol	Cyclo_AVC-PDM
1	Input Voltage	Vs	230 V,50Hz
2	Input Inductance	Li	0.011e-9
3	Load Resistance	R	9.5 Ω
4	Load Resonant Inductance	L	1 mH
5	Load Resonant Capacitance	C	28e-9 F
6	Duty Cycle of MOSFTET	D	Common leg:50 % First leg: 40 %, Second leg: 20 %
9	Switching Frequency	f_{SW}	30kHz
10	Resonant Frequency	f_{reso}	30 kHz

comparing LF modulating wave (2 kHz) with HF carrier wave (30 kHz). The pulse generation circuit of AVC-PDM control is shown in Fig. 2. In order to have Asymmetrical duty cycle for output power control, the pulse width of MOSFET devices used in different legs is given with separate duty. The duty cycle of the common leg devices is set to 50 %.

The devices in the first leg are assigned a 40 % duty cycle, while those in the second leg have a 20 % duty cycle. Whenever the modulating signal goes high pulses are generated, when it goes low pulses are not generated. The Pulse Density Modulation (PDM) control method regulates high frequency currents for induction coil, for regulating the load power. In order to have less switching losses switching frequency (fswit) should be selected slightly higher than or equal to resonant frequency (freso). By controlling the duty period DPDM for signal with small frequency, the change in output power is obtained.

The values of switching frequency and duty cycle for all legs are

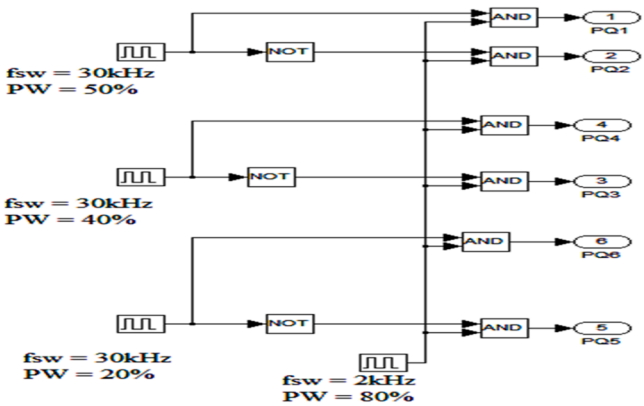

Fig. 2. Pulse generation circuit for AVC-PDM control.

calculated as follows:

Switching frequency,

$$F_s = \frac{1}{T_{Total}} \tag{1}$$

Duty Cycle of common leg,

$$D_{com} = \frac{on - time\ of\ common\ leg}{Total\ time} = \frac{T_{onc}}{T_{Total}} \tag{2}$$

Duty Cycle of first leg,

$$D_{1-leg.AVCPDM} = \frac{on - time\ of\ first\ leg}{Total\ time} = \frac{T_{on1}}{T_{Total}} \tag{3}$$

Duty Cycle of second leg,

$$D_{2-leg.AVCPDM} = \frac{on - time\ of\ second\ leg}{Total\ time} = \frac{T_{on2}}{T_{Total}} \tag{4}$$

The switching pulses for the MOSFET used in the common leg, first leg, and second leg are depicted in Figs. 3, 4, and 5, respectively. Fig. 6 illustrates the output voltage and current through load 1, while Fig. 7 shows the voltage and current through load 2. At lower frequencies, the output voltage may be higher, but the current may also be higher due to lower inductive reactance. This can result in more power being delivered to the load but with less control over the process. At higher frequencies, the output voltage may decrease due to increased inductive reactance, and the current will decrease as well. The system can achieve more precise heating control, but it may require careful management to maintain sufficient power delivery to the load.

Fig. 8 shows the variation in total output voltage with different load resistances, including 7Ω, 8Ω, 9Ω, 10Ω, and 11Ω. As load resistance increases, the output power decreases. Because, in induction heating, power transfer is most efficient when the load and source impedances are closely matched. As the load resistance increases, the impedance mismatch increases, leading to less efficient power transfer, thereby reducing the output power. Fig. 9 depicts the variation of the total output voltage concerning the switching frequency. This study models and simulates the proposed Cyclo-inverter circuit at different frequencies. Operating near the resonant frequency reduces switching losses and improves efficiency. Therefore, selecting a switching frequency slightly higher than the resonant frequency is generally advantageous.

At a switching frequency of 25 kHz, the resonant frequency is lowered. As shown in Fig. 7, at this frequency, the system operates away from resonance, resulting in significant switching losses that lower both output power and efficiency. The source current exhibits high Total Harmonic Distortion (THD), leading to a distorted, non-sinusoidal

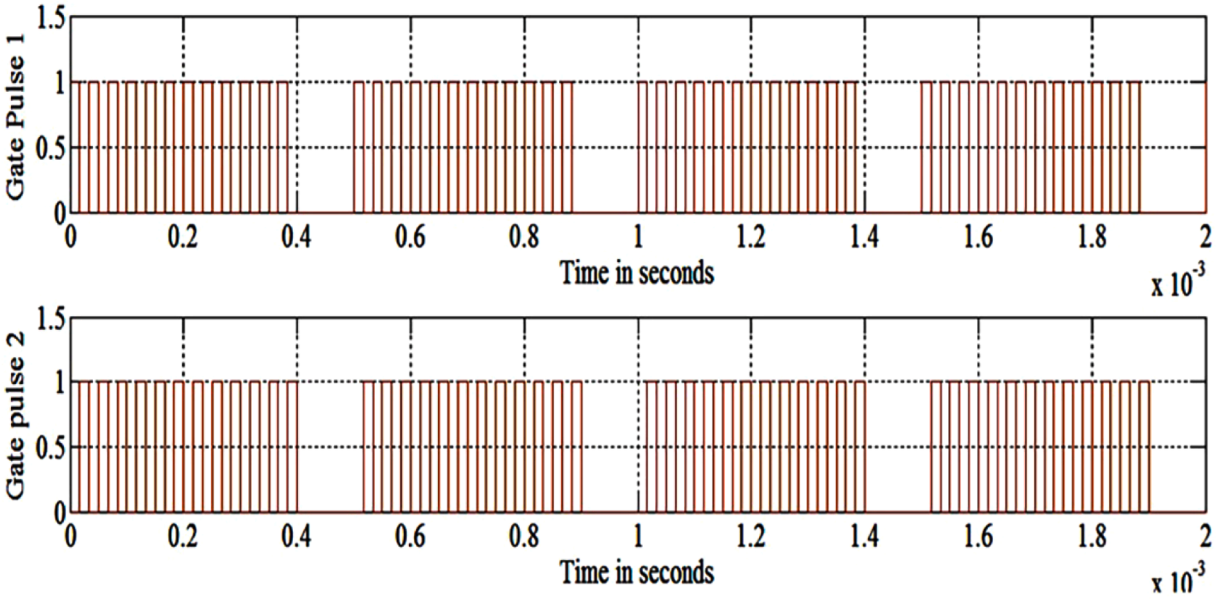

Fig. 3. Switching pulses for common leg devices.

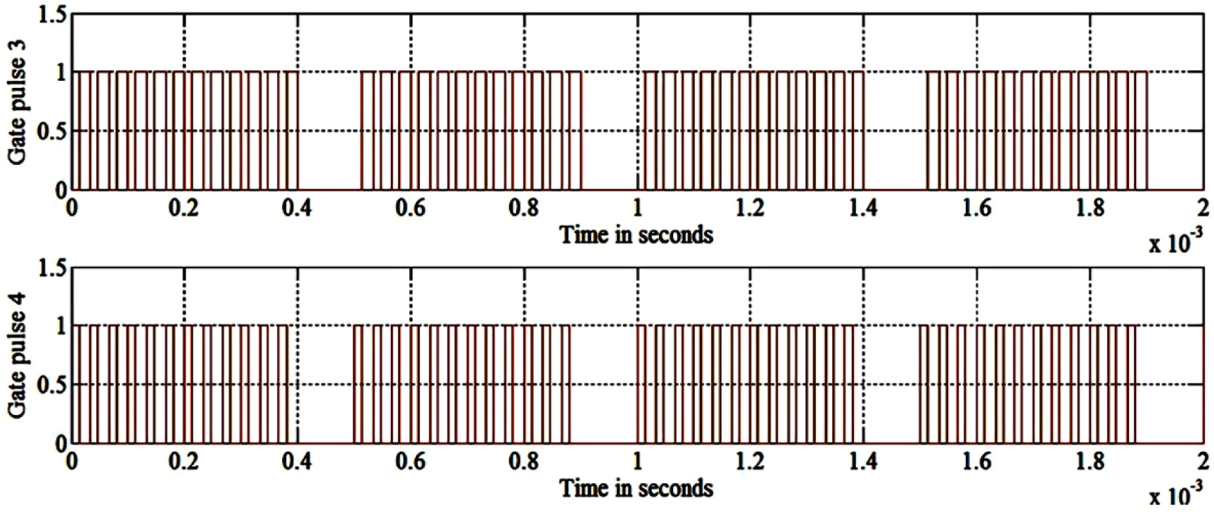

Fig. 4. Switching pulses for devices of leg 1.

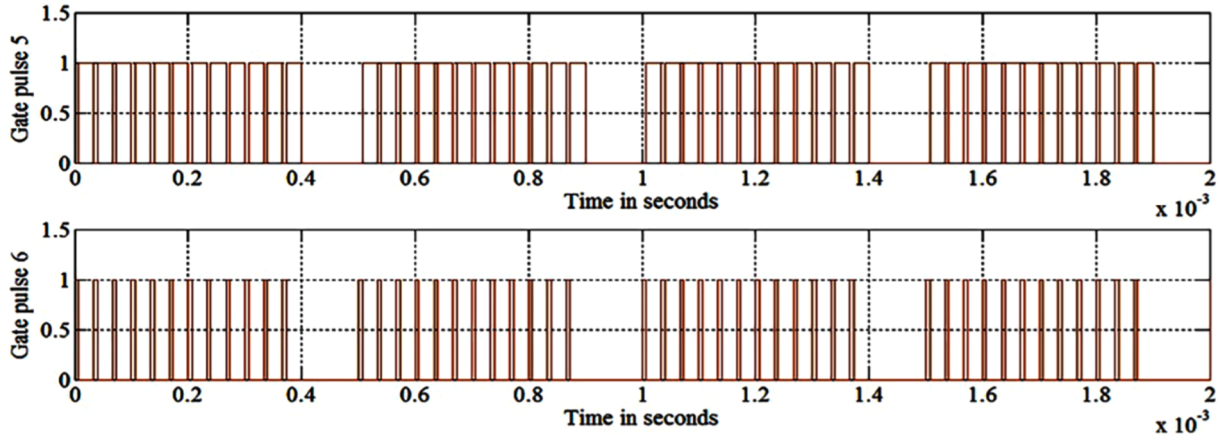

Fig. 5. Switching pulses for devices of leg 2.

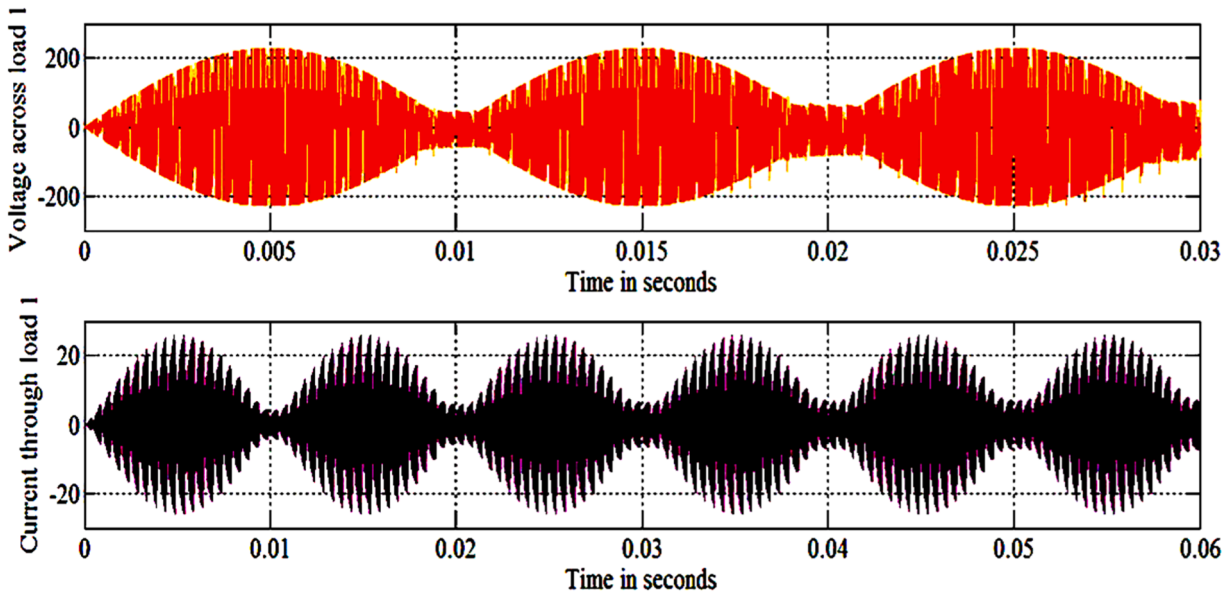

Fig. 6. Voltage across and current through Load 1.

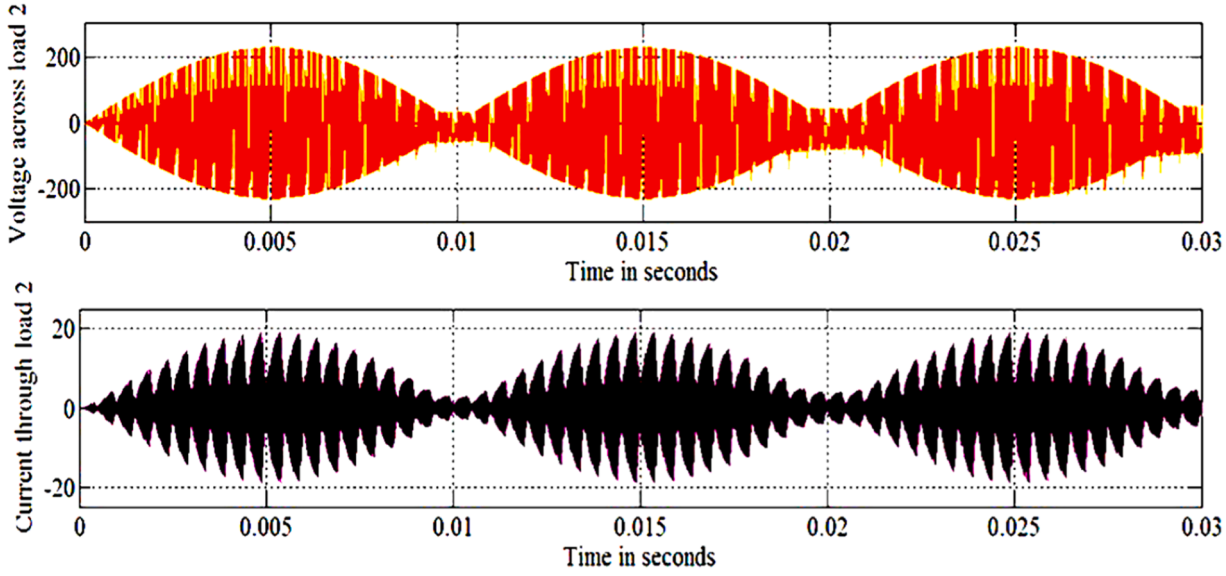

Fig. 7. Voltage across and current through Load 2.

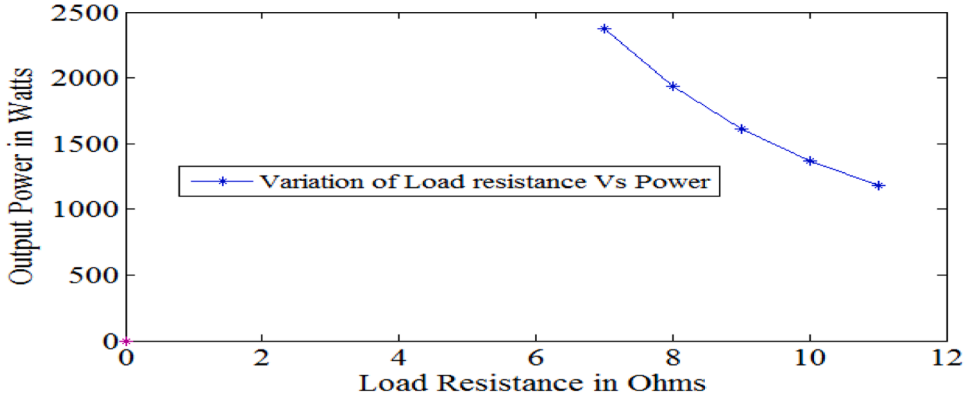

Fig. 8. Variations of total output power with load resistance.

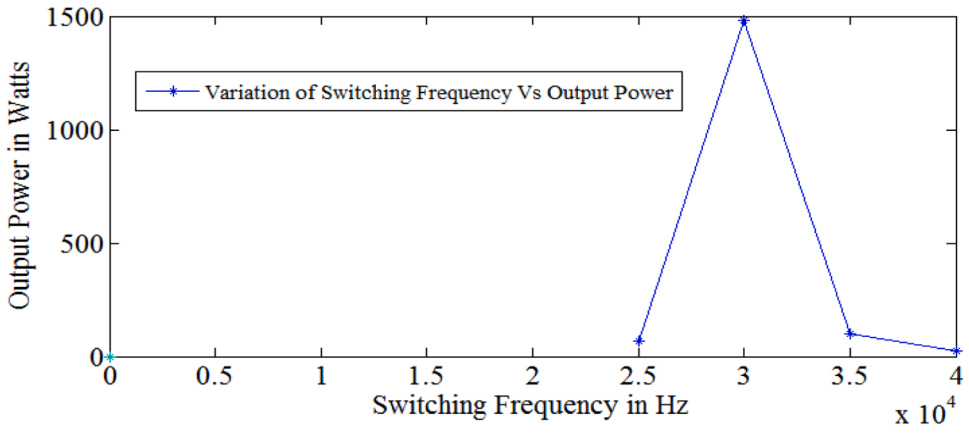

Fig. 9. Variations of total output power with f_{swit}.

waveform and introducing undesirable harmonics into the input voltage. To mitigate these harmonics, an AC filter must be installed on the input side, which adds to the overall cost of the induction heating system. Additionally, a lower switching frequency may generate noticeable perceptible noise. Therefore, using a lower switching frequency is generally avoided.

At a switching frequency of 35 kHz exceeds the resonant frequency, the output current may exhibit a higher Total Harmonic Distortion (THD). This frequency supports induction heating but is not ideal due to detuning from resonance, leading to high switching losses and reduced efficiency. Maximum output power is achieved at 30 kHz, where the load is optimally tuned.

A change in output power with various duty cycles such as 20 %, 30 %, 40 % and 50 % are given in Fig. 10. It shows that as the value of duty ratio is increased, the load power of IH system is also increased. In induction heating (IH) systems, the power supplied to the load is directly related to the amount of energy supplied during each cycle. When the duty ratio is increased, the active period during which power is delivered to the IH load also increases, thereby supplying more energy and increasing the output power. With the chosen values of R_{load} and duty cycles, the changes in total P_{out} is given in Fig. 11. It shows that maximum output power is obtained with maximum duty cycle and the value decreases when the load resistance is increased. Similarly the $f_{switching}$ also affects the output power, especially in applications like induction heating, where the frequency can influence the efficiency of energy transfer. The relationship between switching frequency and output power depends on the specific characteristics of the circuit and load. with the chosen values of load resistance and switching frequency, the variation of total output power is shown in Fig. 12. This implies that the max. P_{output} is achieved with a $f_{switching}$ of 30 kHz, and it decreases as the load resistance increases.

3.2. Open loop system with AVC-PWM control

Asymmetrical Voltage Cancellation-Pulse Width Modulation (AVC-PWM) control is a technique used in IH applications to enhance power efficiency and minimize harmonic distortion. In this approach, Asymmetrical Voltage Cancellation (AVC) adjusts the phase and amplitude of the input voltage to cancel out undesirable voltage components, thereby improving the overall power quality. Pulse Width Modulation (PWM) is then employed to control the duration of the voltage pulses delivered to the induction coil, effectively regulating the power supplied to the system. This combination allows for precise control of the heating process, ensuring stable temperature regulation and efficient power delivery. The AVC-PWM technique improves the system's performance by reducing harmonic interference, enhancing energy efficiency, and providing smoother, more consistent heating in induction heating applications.

According to output power control strategy, Cyclo-inverter fed Induction Heating system is found to be good than other two systems. Now it is required to find the suitable control technique for getting more efficiency from cyclo-inverter fed IH system. Therefore now the Asymmetrical Voltage Cancellation control is combined with Pulse Width Modulation scheme (AVC-PWM) for power control. PWM allows for finer control of the output power by varying the width of the pulses delivered to the load. It can achieve high efficiency and low harmonic distortion, making it suitable for precision heating applications.

The Asymmetrical voltage cancellation concept with Pulse Width Modulation is explained in (Jose M.Burdio 2004) is considered for the simulation. AVC enhances the performance of cycloinverter-fed

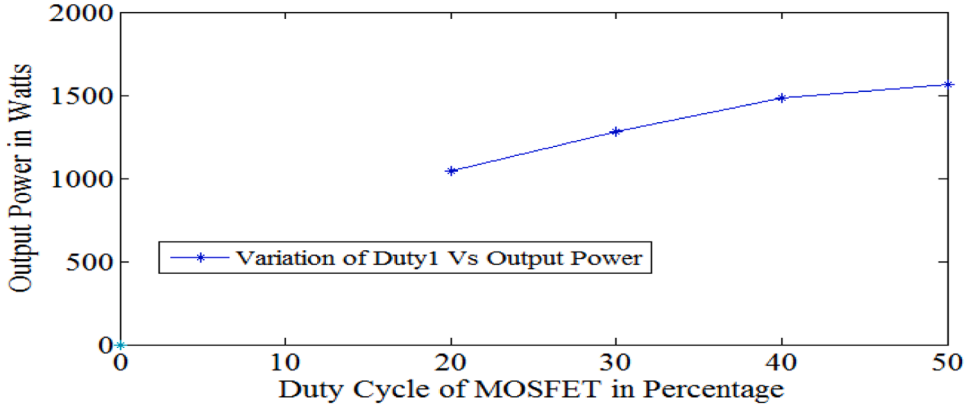

Fig. 10. Variations of total Pout with duty cycle.

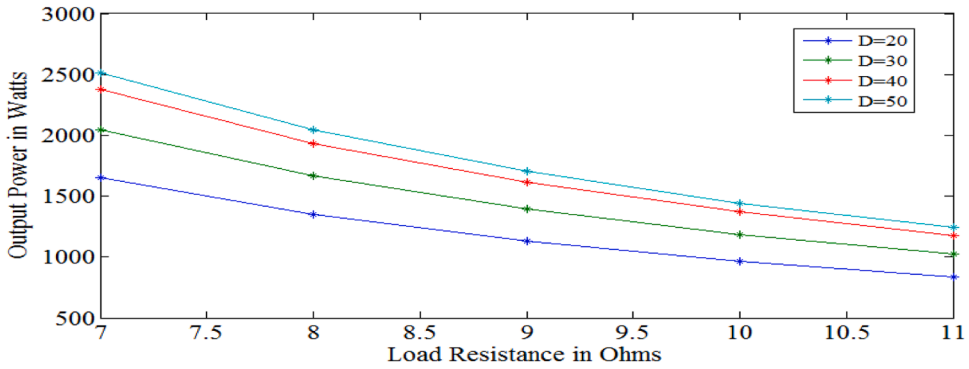

Fig. 11. Variations of total Pout with load resistance and duty cycle.

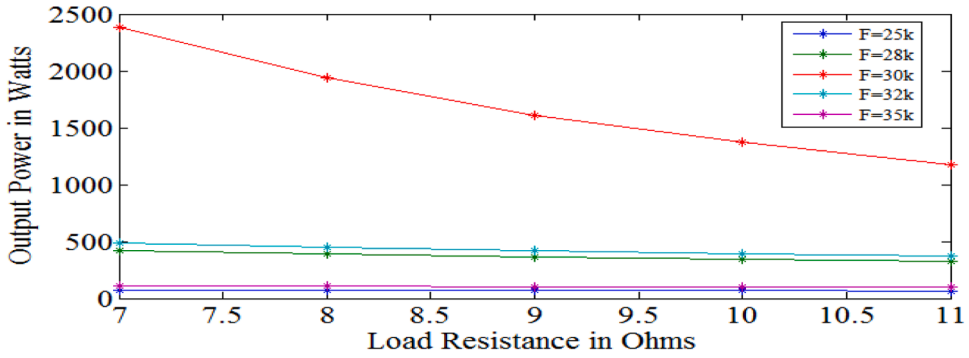

Fig. 12. Variations of total Pout with load resistance and switching frequency.

induction heating systems by improving power control, reducing harmonic distortion, increasing system efficiency, and providing better temperature management while reducing thermal stress and EMI. As stated in Ahmed S.M.W et al. 2009, the values of switching frequency and duty cycle for all legs are calculated as follows:

Duty Cycle of common leg,

$$D_{com} = \frac{on - time\ of\ common\ leg}{Total\ time} = \frac{T_{onc}}{T_{Total}} \quad (5)$$

Duty Cycle of first leg,

$$D_{1-leg,\ AVCPWM} = \frac{on - time\ of\ first\ leg}{Total\ time} = \frac{T_{on1}}{T_{Total}} \quad (6)$$

Duty Cycle of second leg,

$$D_{2-leg.AVCPWM} = \frac{on - timeofsecondleg}{Totaltime} = \frac{T_{on2}}{T_{Total}} \quad (7)$$

Pulse generation circuit and its waveform for AVC-PWM control is shown in Figs. 13 and 14 respectively. The gate pulses for six MOSFET's used in high frequency inverter circuit is generated by considering unequal pulse width in all the three legs. A 30 kHz high frequency signal with 50 % pulse width for common leg, 40 % pulse width for second leg and 20 % pulse width for third leg is considered in this work. This control voltage has four control variables such as control angles (α+, α- and β) & the switching period (Ts).

In fixed frequency control, the switching period (Ts) remains constant, resulting in the use of only three control variables. Consequently, the control policy utilizing control functions α+, α-, and β is referred to as asymmetrical voltage-cancellation control. When β is fixed at 180°, variations in the load voltage and power are achieved by separately adjusting the control functions α+ or α-.

Figs. 15, 16, and 17 show the switching pulses for the MOSFETs in the common leg, I leg and II leg, respectively. Figs. 18 and 19 display the output voltage and current for load 1 and load 2, respectively. The

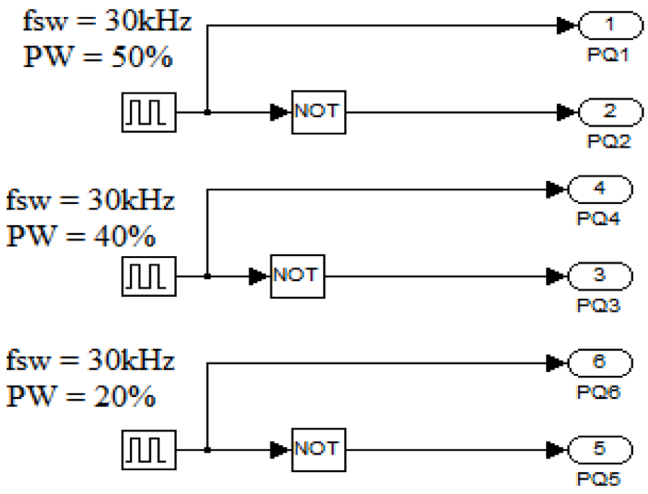

Fig. 13. Control circuit for AVC-PWM control.

amplitude of voltage and current waveforms are symmetrical only under resonance condition. Other than resonance, the upper and lower magnitude of current and voltages are unsymmetrical.

Maximum heat is obtained only when large amount of eddy current flows through induction coil. This is possible only at resonance condition. In order to verify this fact, the circuit is simulated for various load resistances like 7Ω, 8Ω, 9Ω, 10Ω & 11Ω, various switching frequencies like 25 kHz, 30 kHz, 35 kHz and various duty cycles like 20 %, 30 %, 40 % and 50 % and the results are presented. Changes in total P_{out} with various R_{load} is shown in Fig. 20. Lower resistance increases output power, but can cause efficiency issues at extremes.

Changes in total P_{out} with various F_{swit} is shown in Fig. 21. Higher frequencies generally increase power but must balance with switching

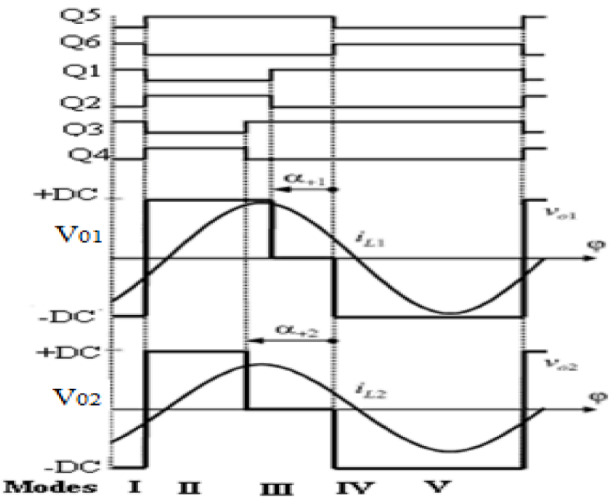

Fig. 14. Characteristic waveforms of AVC-PWM control for inverter.

losses and desired heating depth. Fig. 22 illustrates the variation in total output power with different duty cycles. Higher duty cycles increase output power and allow for fine control over heating intensity. Fig. 23 shows the changes in total Pout with various load resistances and duty cycles. Changes in total P_{out} with various load resistance and switching frequency is shown in Fig. 24.

Performance plot indicates that the total Pout increases with increase in duty cycle and decreases with increase in load resistance. The output voltage to the load increases with the duty ratio. A higher duty cycle raises the average voltage, increasing the current and output power. And the load parameters are tuned to the switching frequency of 30 kHz hence except this frequency the output power decreases. At 30 kHz frequency, the interaction between the coil and the workpiece generates an optimal electromagnetic field that produces the desired heating effect. The coil's inductance and the capacitive network (or other circuit elements) are matched to this frequency. Running at the resonant frequency reduces the impedance observed by the inverter, allowing more current to flow and hence delivering more power to the load.

4. Fourier analysis

Under steady-state conditions, the output voltage of inverters is a periodic function of time. This periodic function can be described using a constant term along with an infinite series of sine and cosine functions of time through Fourier analysis [14]. Output voltage wave shape of Full bridge Series Resonant Inverter differs from Cyclo-inverter topologies due to the type of input which is applied to the inverter. Former is

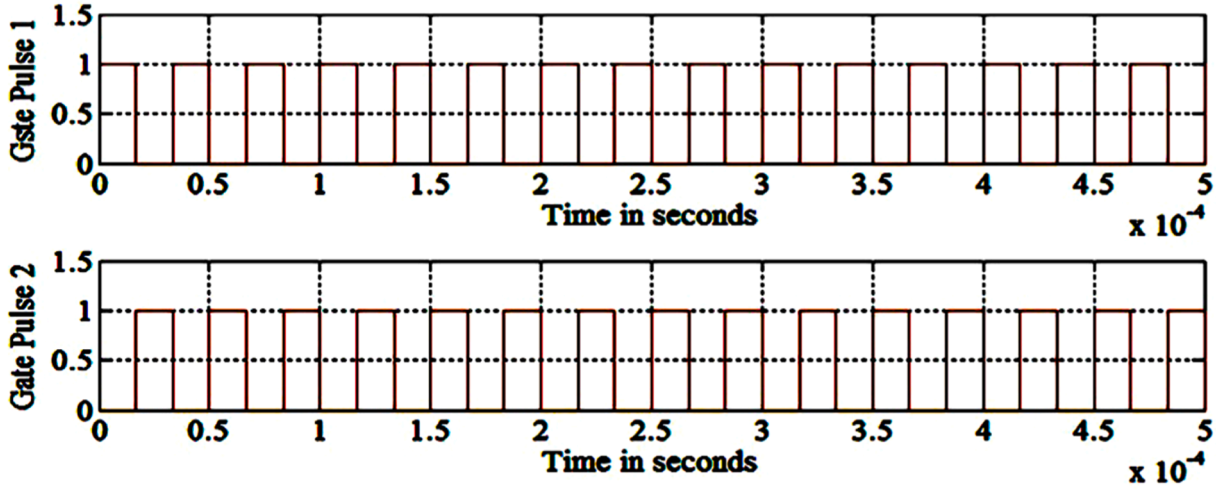

Fig. 15. Switching pulses for common leg devices.

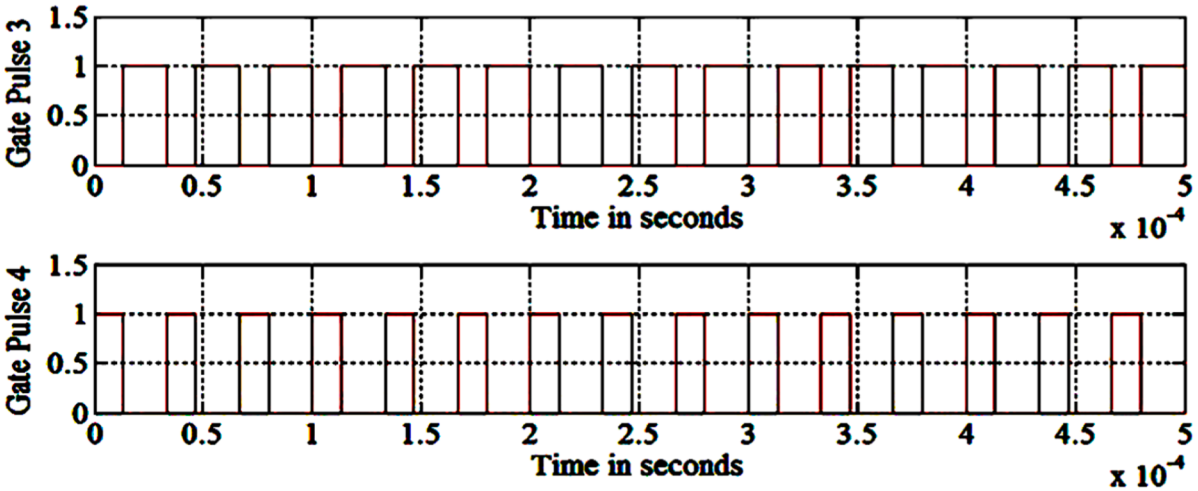

Fig. 16. Pulse switching for devices in leg 1.

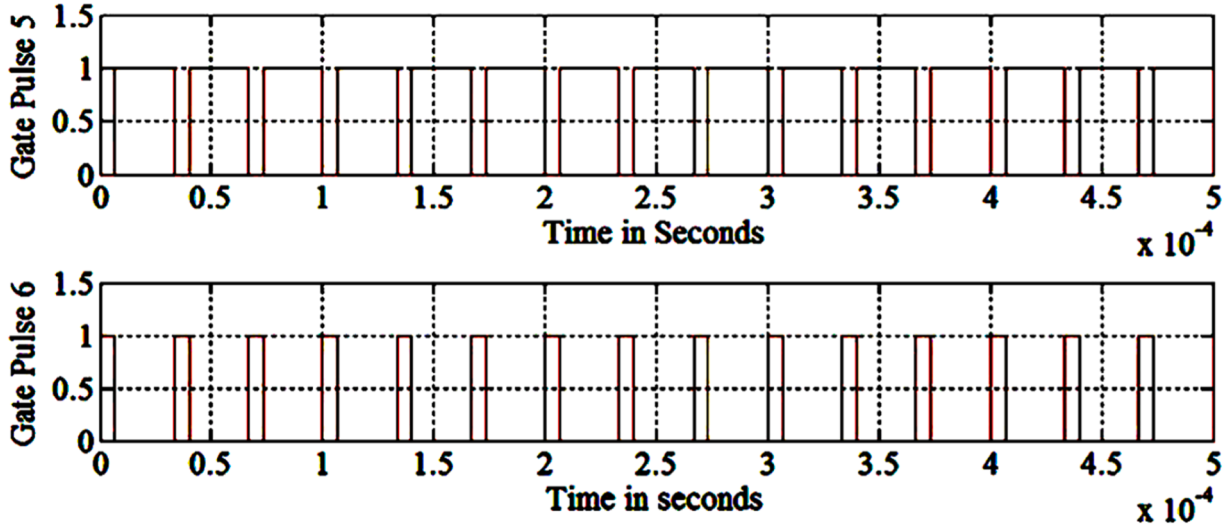

Fig. 17. Pulse switching for devices in leg 2.

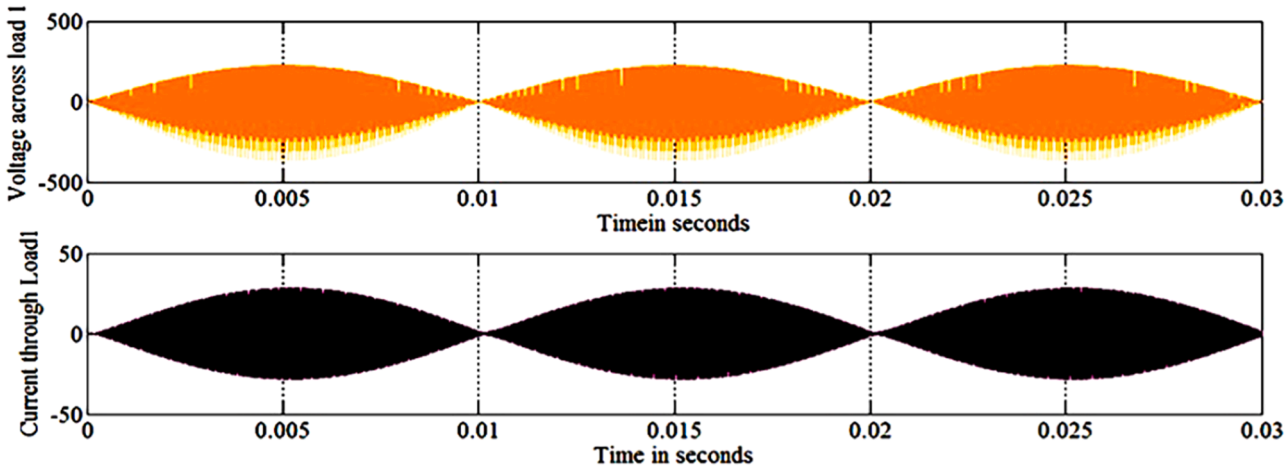

Fig. 18. Output voltage and current in load 1.

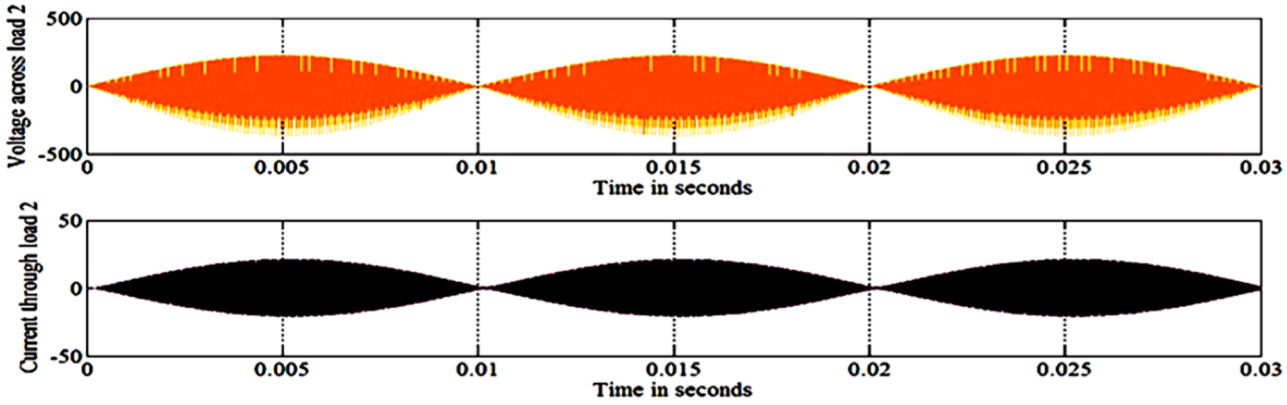

Fig. 19. Output voltage and current in Load 2.

supplied with pure DC input whereas later with pulsating DC input.

i) **Fourier Analysis of Inverter Output when the Input is Pure DC**

The output voltage wave shape of series resonant inverter with AVC-PWM technique is shown in Fig. 25 below. The output voltage V_{o_dc} can be expressed as,

$$V_{o\_dc} = V_{dc} + \sum_{n=1}^{\infty} V_{an}\cos n\omega_s t + V_{bn}\sin n\omega_s t \quad (8)$$

where, V_{dc} is the DC component of output voltage

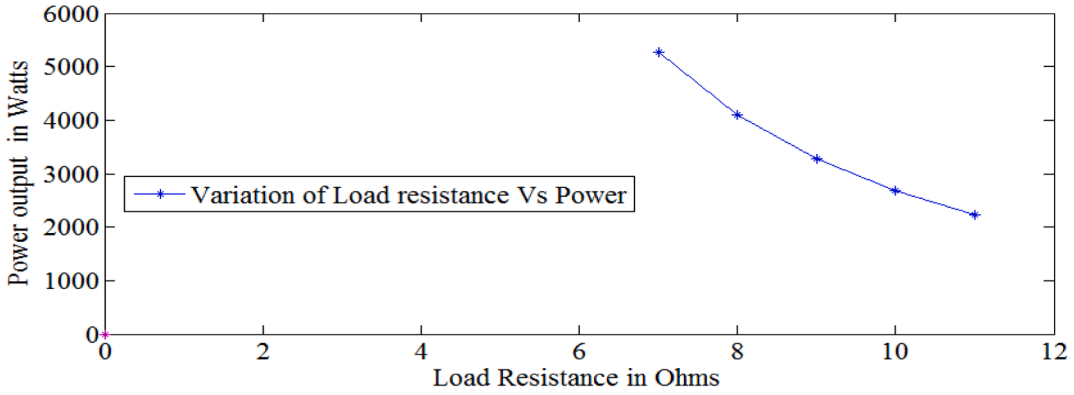

Fig. 20. Variations of total output power with load resistance.

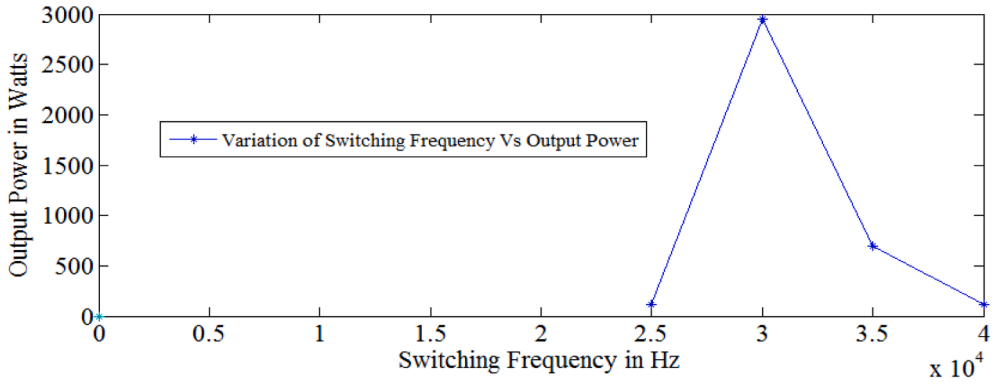

Fig. 21. Variations of total output power with switching frequency.

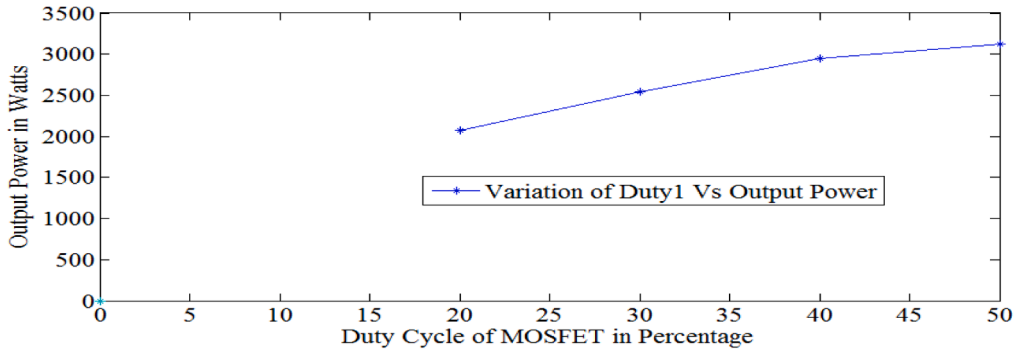

Fig. 22. Variations of total output power with duty cycle.

V_{an} and V_{bn} are constants.

The equation of $V_{o\text{-}dc\_}$ is given by,

$$V_{o\_dc} = \begin{cases} +V_d; 0 \le \vartheta \le (\pi - \varphi) \\ 0; (\pi - \varphi) \le \vartheta \le \pi \\ -V_d;\ \pi \le \vartheta \le 2\pi \end{cases} \quad (9)$$

The Fourier representation of $V_{0\text{-}dc}$ is derived as shown below:

Fourier coefficient, a_0

In general,

$$a_0 = \frac{2}{T}\int_0^T x(t)dt \quad (10)$$

Here, $T = 2\pi$; $x(t) = V_{0\text{-}dc}$

$$a_0 = \frac{2}{2\pi}\int_0^{2\pi} V_{o\_dc}d\theta$$

$$= \frac{1}{\pi}\int_0^{\pi-\varphi} V_d\, d\theta + \frac{1}{\pi}\int_{\pi-\varphi}^{\pi} 0 \times d\theta + \frac{1}{\pi}\int_{\pi}^{2\pi} (-V_d)d\theta$$

$$= -\frac{V_d\phi}{\pi}$$

$$DC\ component,\ V_{dc} = \frac{a_0}{2} = -\frac{V_d\phi}{2\pi} \quad (11)$$

Fourier Coefficient, a_n

In general,

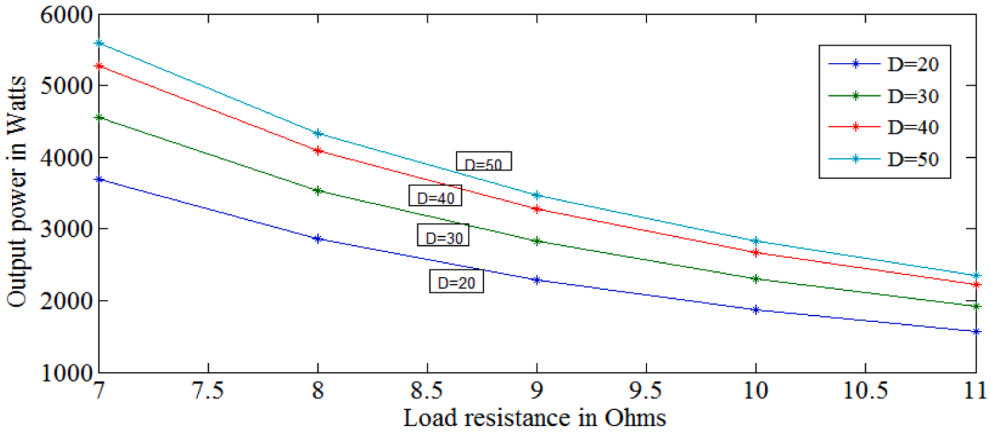

Fig. 23. Variations of total Pout with load resistance and duty cycle.

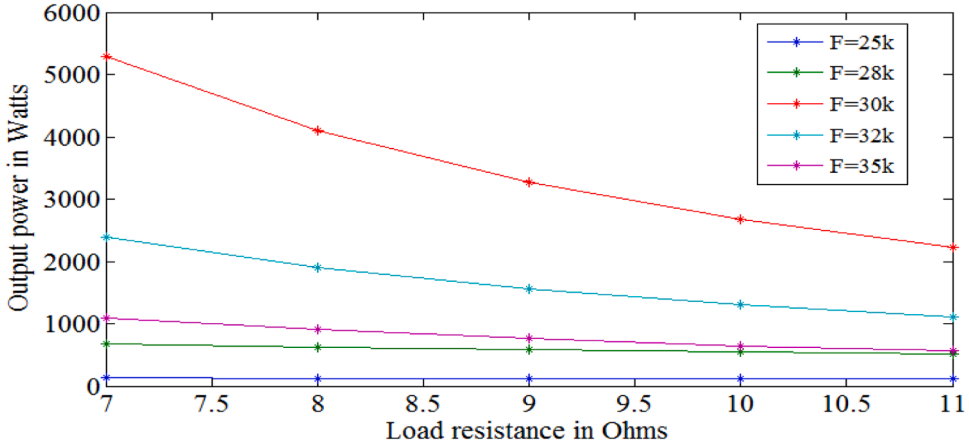

Fig. 24. Variations of total Pout with load resistance and switching frequency.

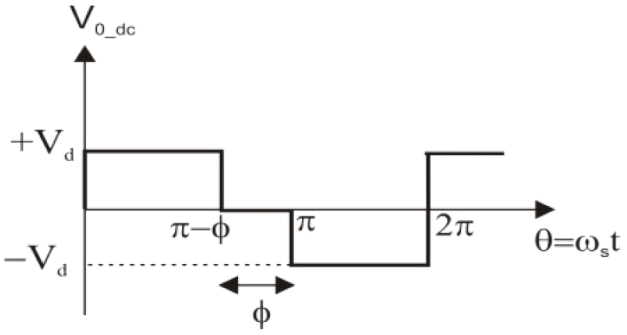

Fig. 25. Output Voltage Wave Shape of SRI.

$$a_n = \frac{2}{T}\int_0^T x(t)cosn\Omega_o t dt \tag{12}$$

Here, $T = \pi$; x(t) = $V_{0\text{-}dc}$, $\Omega_0 t = \theta_0$ $\theta = \omega t$ $\theta = \omega_s t$ $n\theta_0 = n\omega_s t$

$$\therefore a_n = \frac{2}{2\pi}\int_0^{2\pi} V_{o\_dc}\ cosn\theta_0 d\theta$$

$$= \frac{V_d}{\pi n}\sin n(\pi - \phi)$$

Cosine Component

In general,

$$\text{Cosine component of Fourier series } = \sum_{n=1}^{\infty} a_n cosn\Omega_0 t$$

Here, $\Omega_0 = \omega_s$

$$\therefore \text{Cosine component} = \sum_{n=1}^{\infty}\frac{V_d}{\pi n}\sin n(\pi - \phi)cosn\omega_s t$$

$$= \sum_{n=1}^{\infty} V_{an}cosn\omega_s t$$

Where

$$V_{an} = \frac{V_d}{\pi n}\sin n(\pi - \phi) \tag{13}$$

Fourier Coefficient, b_n

$$b_n = \frac{2}{T}\int_0^T x(t)\sin n\Omega_o t\ dt \tag{14}$$

$$b_n = \frac{2}{2\pi}\int_0^{2\pi} V_{o\_dc}\sin n\theta_o d\theta$$

$$= \frac{1}{\pi}\int_0^{\pi-\phi} V_d \sin n\theta_0 d\theta + \frac{1}{\pi}\int_{\pi}^{2\pi}(-V_d)\sin n\theta_0\ d\theta$$

$$= -\frac{V_d}{n\pi}\cos n(\pi-\phi) + \frac{2V_d}{n\pi} - \frac{V_d \cos n\pi}{n\pi}$$

Sine Component

In general,

$$\text{Sine Component of Fourier series} = \sum_{n=1}^{\infty} b_n \cos n\Omega_0 t$$

$$\therefore \text{Sine Component} = \sum_{n=1}^{\infty}\left(-\frac{V_d}{n\pi}\cos n(\pi-\phi) + \frac{2V_d}{n\pi} - \frac{V_d\cos n\pi}{n\pi}\right) sinn\omega_s t$$

$$= \sum_{n=1}^{\infty} V_{bn} \sin n\omega_s t$$

Where,

$$V_{bn} = -\frac{V_d}{n\pi}\cos n(\pi-\phi) + \frac{2V_d}{n\pi} - \frac{V_d\cos n\pi}{n\pi} \quad (15)$$

Now, the Fourier series representation of V_{o_dc} is given by,

$$V_{o\_dc} = V_{dc} + \sum_{n=1}^{\infty} V_{an}\cos n\omega_s t + V_{bn} sinn\omega_s t \quad (16)$$

Where,

$$V_{dc} = -\frac{V_d\phi}{2\pi}$$

$$V_{an} = \frac{V_d}{\pi n}\sin n(\pi-\phi)$$

$$V_{bn} = \frac{V_d}{\pi n}\cos n(\pi-\phi) + \frac{2V_d}{n\pi} - \frac{V_d cos n\pi}{n\pi}$$

i) **Fourier Analysis of Inverter Output when the Input is Rectified AC**

The output voltage wave shape of Cyclo-inverter with AVC-PWM technique is shown in Fig. 26 below.

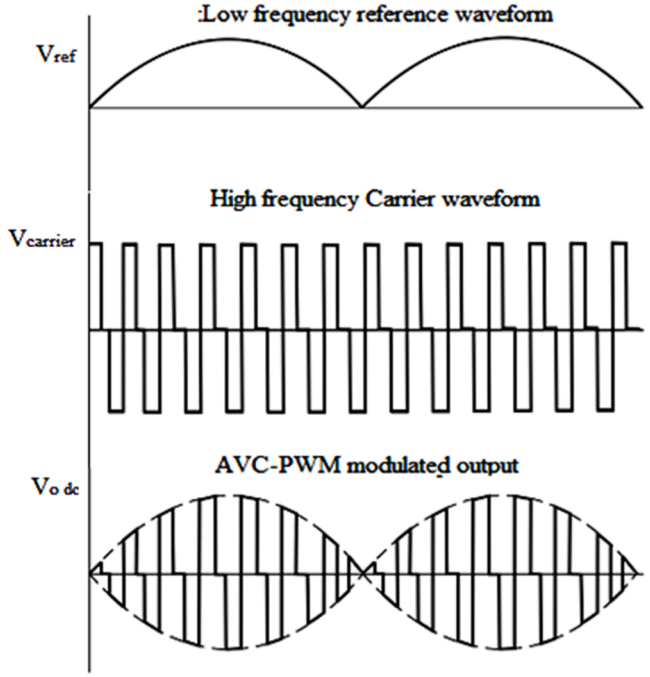

Fig. 26. Output voltage wave shape of Cyclo-inverter.

The Fourier representation of $V_{0\text{-ac}}$ is derived from the result of previous analysis as shown below:

Now, the Fourier series representation of V_{o_ac} is given by,

$$V_{o\_ac} = V_{o\_dc}\ V_m\ sin\ w\ t \quad (17)$$

i) **Analysis of output voltage**

With reference to literature survey, the quasi square wave output voltage for each output controlled by adjusting phase-shift angle φ, on positive side can be expressed by a Fourier series,

$$V_0 = V_{dc} + \sum_{n=1}^{\infty}(V_{an}\cos n\omega_s t + V_{bn}\sin n\omega_s t) \quad (18)$$

and rms value of output voltage is given by,

$$V_{0,rms} = \sqrt{\sum_{n=1}^{\infty} V_{n,rms}^2} = \sqrt{V_{dc}^2 + \sum_{n=1}^{\infty}\left(\frac{V_n}{\sqrt{2}}\right)^2} \quad (19)$$

Where

$$V_n = \sqrt{V_{an}^2 + V_{bn}^2} \quad (20)$$

i) **Analysis of output current**

The resonant load current is drawn from a DC link through a full bridge inverter whose waveform is like a sinusoidal waveform causing from an RLC series resonant load. The equation of resonant load current can be analyzed by superposition theorem and Fourier series.

The resonant load current is given by,

$$i_0 = I_{dc} + \sum_{n=1}^{\infty}(I_{an}\cos n\omega_s t + I_{bn}\sin n\omega_s t) \quad (21)$$

And the RMS value of output voltage is given by,

$$I_{0,rms} = \sqrt{\sum_{n=1}^{\infty} I_{n,rms}^2} = \sqrt{I_{dc}^2 + \sum\left(\frac{I_n}{\sqrt{2}}\right)^2} \quad (22)$$

Where

$$I_n = \sqrt{I_{an}^2 + I_{bn}^2} \quad (23)$$

i) **Analysis of output power**

The output power can be calculated by the summation of all harmonic frequency rms voltages which are multiplied by all harmonic frequency rms currents.

$$P_{total} = P_{0,Load1} + P_{0,Load2} \quad (24)$$

$$P = \sum_{n=1}^{\infty} V_{n,rms} I_{n,rms}\cos\theta_n \quad (25)$$

5. Control technique comparison

The Cyclo-inverter topology is analyzed with two control techniques such as AVC-PDM and AVC-PWM by considering same simulation parameters, now the comparisons is made on these two techniques based on the following parameters for output power control in order to identify the best technique for Cyclo-inverter fed induction heating system. While AVC, PDM, and PWM have been explored individually, their integration in the context of Cyclo-inverter-fed Induction Heating (IH) systems for precise output power control is novel. This combination provides enhanced flexibility and control compared to traditional

methods. Fourier analysis of the output voltage, which is not commonly addressed in prior works. This analysis provides a deeper understanding of the harmonic performance and effectiveness of the proposed techniques.

Fig. 27 shows the parameters used for control technique comparison of Cyclo-inverter fed IH system. Table 2 shows the control technique comparison for Cyclo-inverter fed IH system. It indicates that maximum efficiency with minimum THD on supply current is obtained in AVC-PWM based Cyclo-inverter fed IH system.

The focus of this work is on achieving high power and energy efficiency in Cyclo-inverter-fed Induction Heating systems. The proposed techniques successfully deliver efficiencies of over 93 %, which is a critical requirement for many practical applications.

In induction heating applications, especially in industrial and domestic environments, achieving precise power control and efficiency often takes precedence over minimizing THD. Harmonic distortion is inherently higher in systems operating with modulation techniques like AVC, and the system design compensates for this in specific use cases. Although the presented results focus on the control techniques, future work can integrate filtering techniques or circuit modifications to reduce THD further without compromising efficiency.

Despite the observed THD values, the proposed techniques offer improved control flexibility and better energy utilization compared to traditional methods, as demonstrated in the results.

6. Transient response analysis and PF improvement

Many domestic and industrial appliances now use Fuzzy Logic Control (FLC) systems, a non-linear approach to improve inverter output and system dynamics. The centroid defuzzification technique adjusts the inverter's power output based on the operator-set reference value. Professional understanding is necessary in designing the fuzzy based control system and it is best suited for the scheme with huge deviation in input and output parameters. Because this controller is forceful to variations in input and output parameters. The main advantage of this technique is that it doesn't need a mathematical model like traditional systems, but requires a clear understanding of the process and control needs. The user defines the data flow, which is then processed to generate the corresponding output.

The design of FLC involves 3 steps. They are Fuzzification, Knowledgebase and Defuzzification. Fuzzification converts measured crisp values into fuzzy variables, Knowledge base is nothing but the reasoning mechanism defined by the experts and finally the conversion of fuzzy variables into crisp value is called defuzzification mechanism. Sugeno Fuzzy Models is preferred for this application because it generates fuzzy rules from a given input-output data set. The duty cycle of inverter switches are altered in accordance with the signal obtained from FLC. The FLC based Cycloinverter is simulated with MATLAB simulink Fuzzy toolbox. PQ block measures the actual power output and then it is compared with set power defined by the user. The output of the comparator gives an error signal. The error signal and its derivative in power form the input to the FLC and the control signal obtained from FLC is considered as output.

The Fuzzy Logic Controller takes two inputs (Error and Change in error) and one output, represented by five triangular functions as given in Figs. 28, 29 and 30 respectively. The FLC rule base and surface plot depicting the relationship between error, change in error, and output power are provided in Table 3 and in Fig. 31 respectively with inverter switching pulses adjusted to match the set power. Figs. 32, 33 and 34 shows the RMS voltage, current, and mean power waveforms for a 60 W set power respectively.

The transient parameters for the cyclo-inverter fed induction heating (IH) system controlled by fuzzy logic (FL) controllers are as follows: The system demonstrates a rapid transient response, achieving a settling time of 0.08 s, which indicates the time taken to reach and remain within the desired output power range. The system exhibits excellent

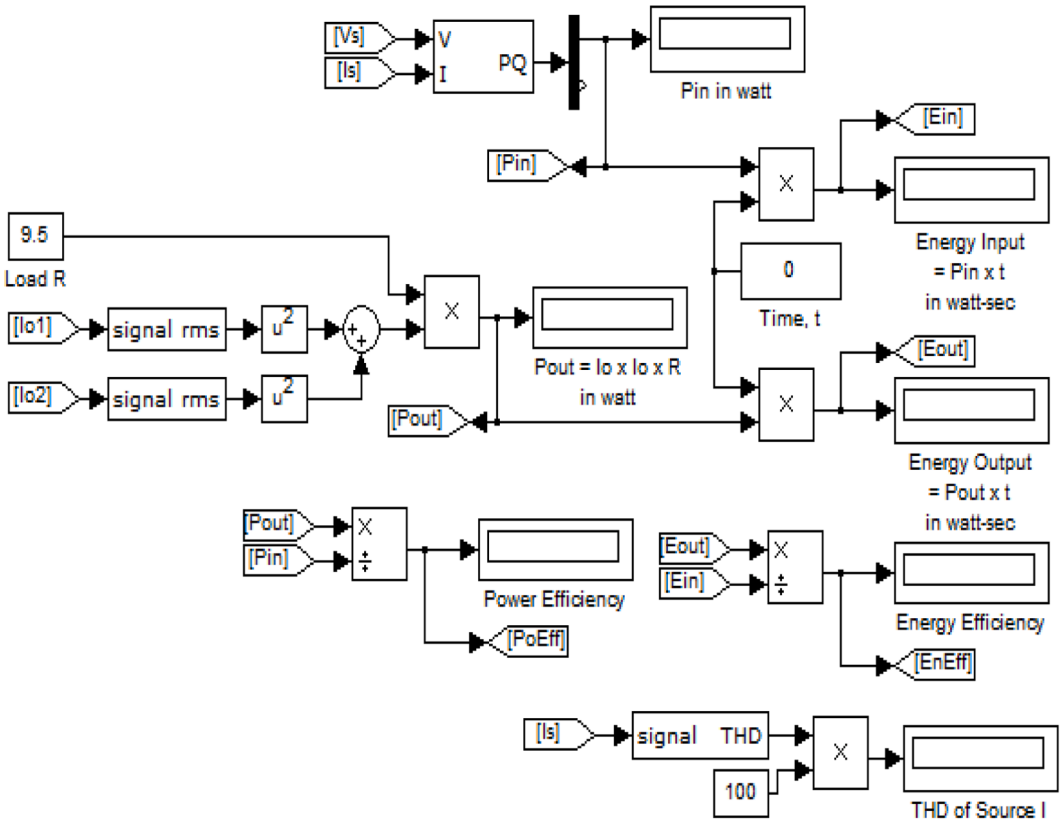

Fig. 27. Parameters for control technique comparison.

Table 2
Control technique comparison for Cyclo-inverter fed IH system.

Control Technique	Pin Watts	Pout Watts	Power Efficiency %	Ein J/ Sec	Eout J/ Sec	Energy Efficiency %	THD %
AVC-PWM	3148	2952	93.75	3148	2952	93.75	56.34
AVC- PDM	2302	2134	92.73	2302	2134	92.73	82.81

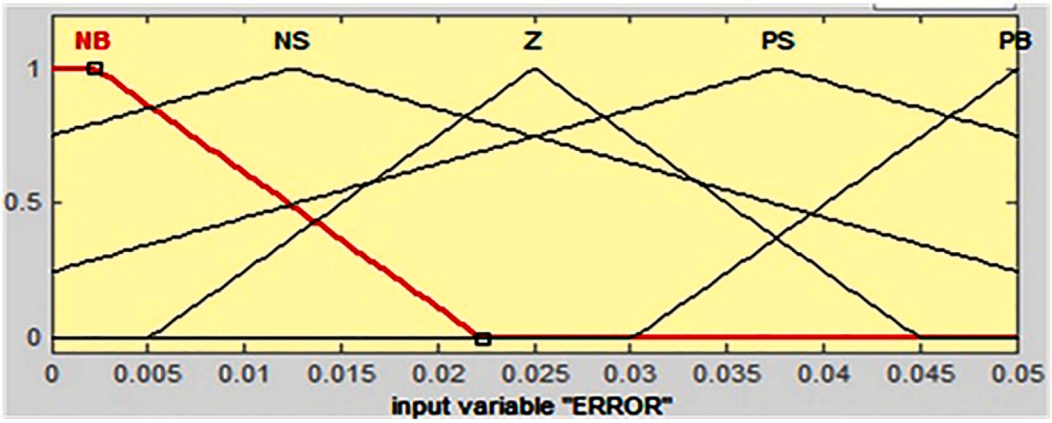

Fig. 28. Triangular membership function for error.

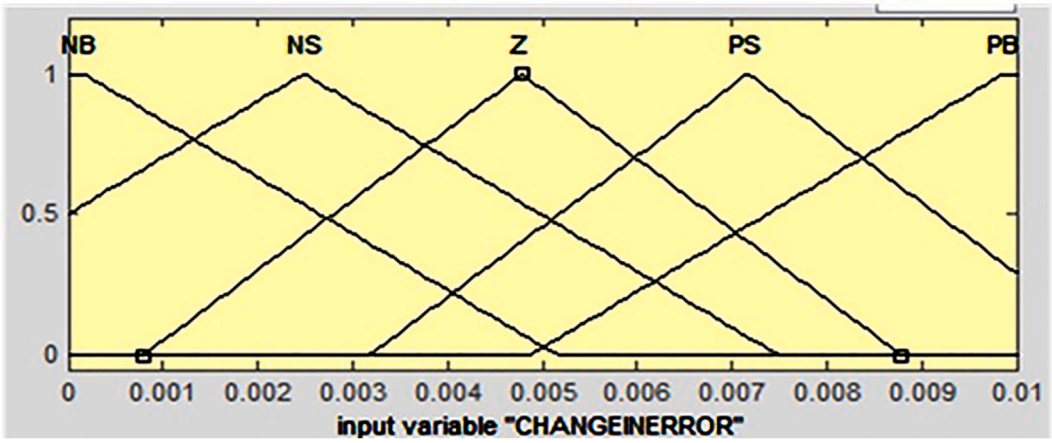

Fig. 29. Triangular membership function for change in error.

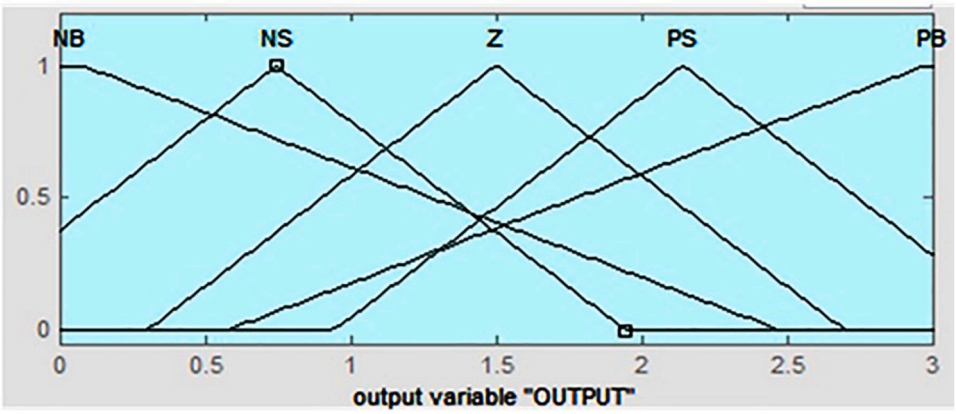

Fig. 30. Triangular membership functions for control output.

Table 3
Rule base used for FLC.

e /Δe	NB	NS	Z	PS	PB
NB	Z	PS	PB	NB	NS
NS	PB	Z	NB	PS	NS
Z	NB	NS	Z	PS	PB
PS	NB	NS	PB	Z	PS
PB	NS	PB	NB	PS	Z

steady-state performance with a steady-state error of 0.01 Watts, ensuring precise power regulation and achieving the desired output power without deviations.

Cyclo-inverter topologies without DC link capacitors generate significant harmonics on the AC supply, which can negatively affect systems sharing the same bus bar. In conventional full-bridge Resonant Inverter designs, these harmonics disrupt DC link capacitor operation. To mitigate these effects, the cyclo-inverter-based Induction Heating System (IHS) incorporates input filters like L-filters, T-filters, and boost converters to enhance the input power factor. Among these, the boost converter has demonstrated superior performance. Simulations of the proposed circuit confirm its effectiveness. Basic cyclo-inverter designs often exhibit a low power factor (PF) due to a large PF angle. Adding a boost converter on the input side improves PF, while diode bridge rectifiers, commonly used for AC line operation, achieve a PF of 0.9 with resistive loads but lower values with inductive loads. Fig. 35 illustrates the combined boost converter and cyclo-inverter configuration for the

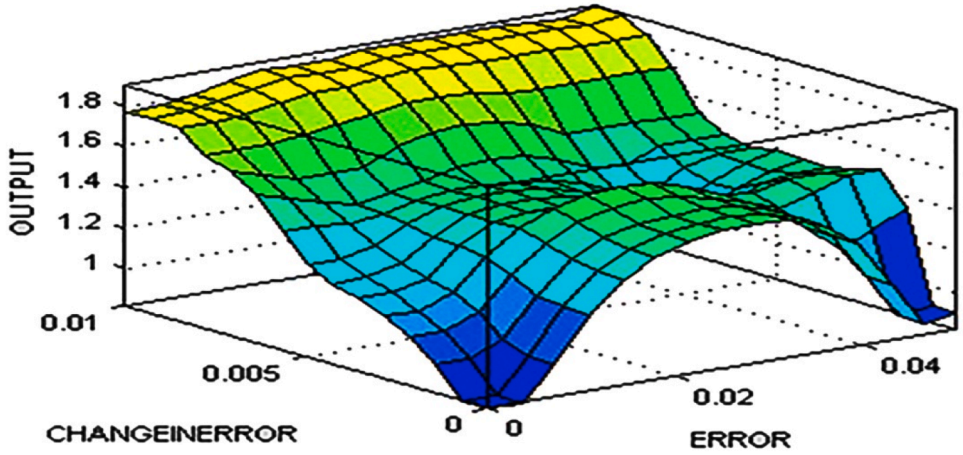

Fig. 31. Surface plot.

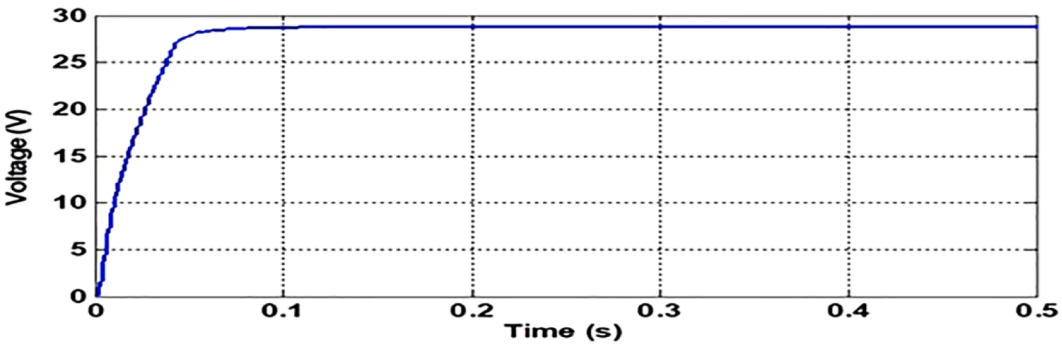

Fig. 32. RMS voltage waveform for a reference power of 60W.

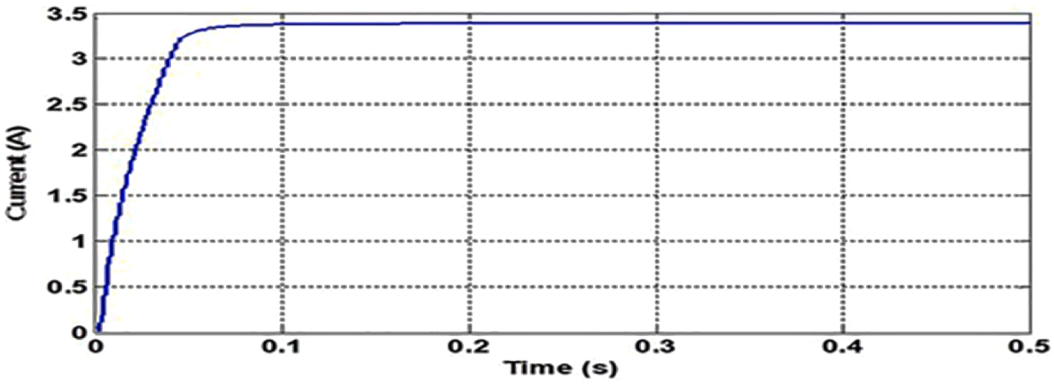

Fig. 33. RMS current waveform for a reference power of 60W.

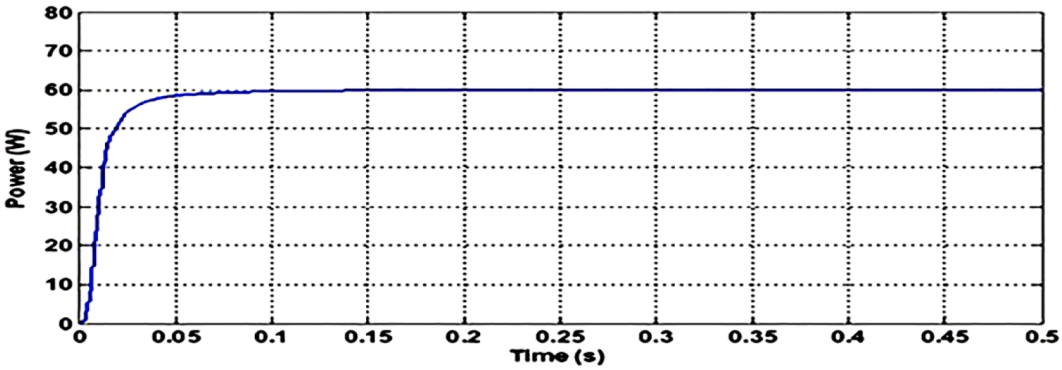

Fig. 34. Average power waveform for 60 W.

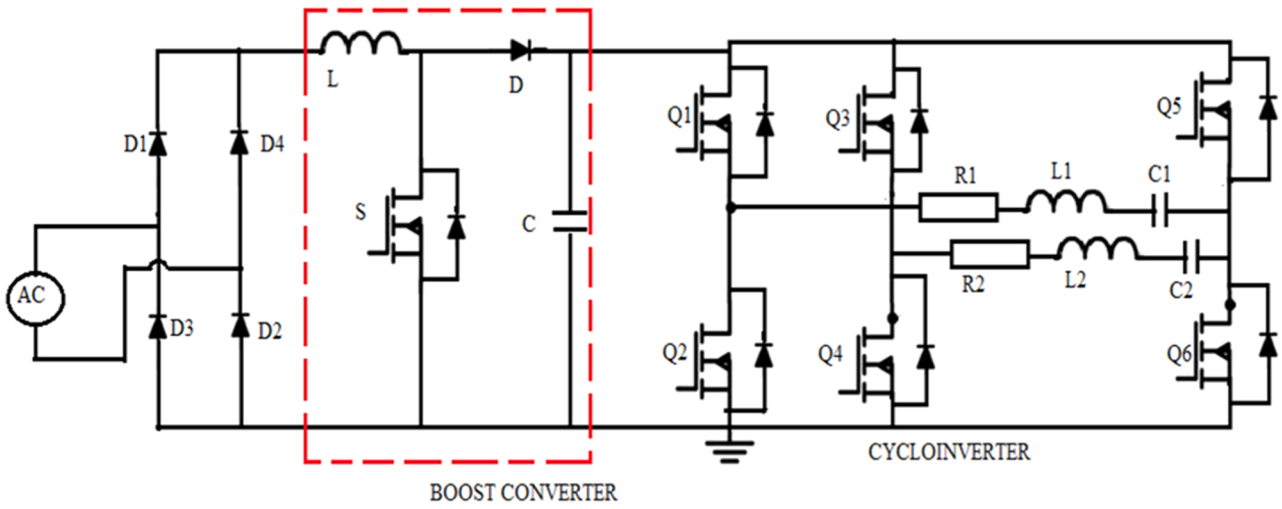

Fig. 35. Cyclo-inverter circuit with Boost converter.

IH system.

The waveforms of input parameters are shown in Fig. 36. From this waveform it is observed that PF is close to unity. The frequency Spectrum of a Cyclo-inverter fed IH system with Boost converter is shown in Fig. 37, which produces a distortion of 4.48 %.

The performance metrics of the cyclo-inverter fed IH system integrated with a boost converter for power factor correction (PFC) are as follows: The phase angle is 5.4°, indicating minimal lag between voltage

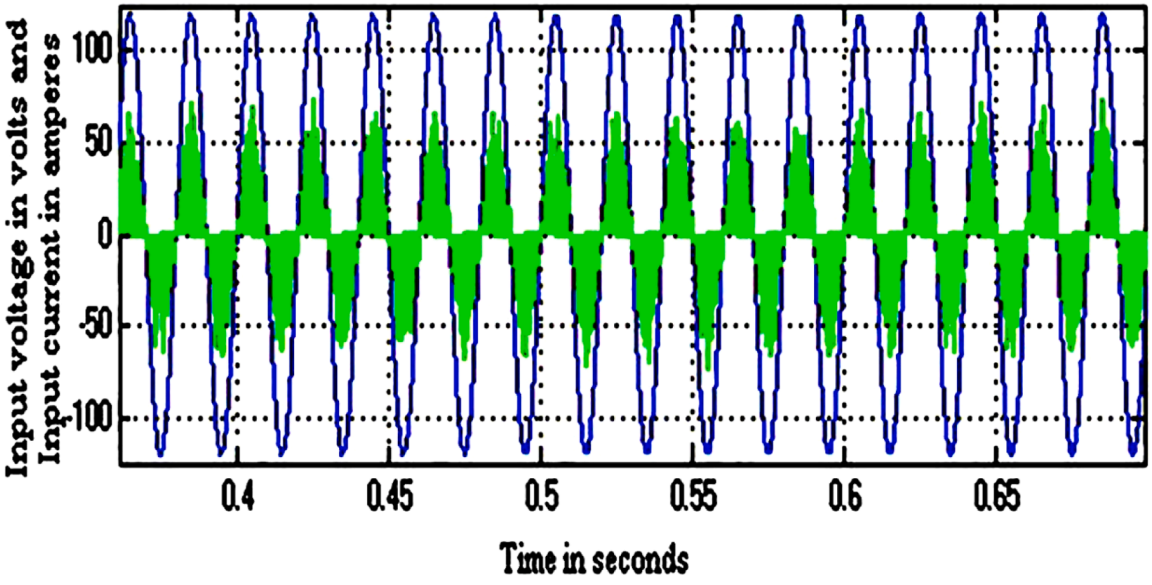

Fig. 36. Waveforms of input V and I.

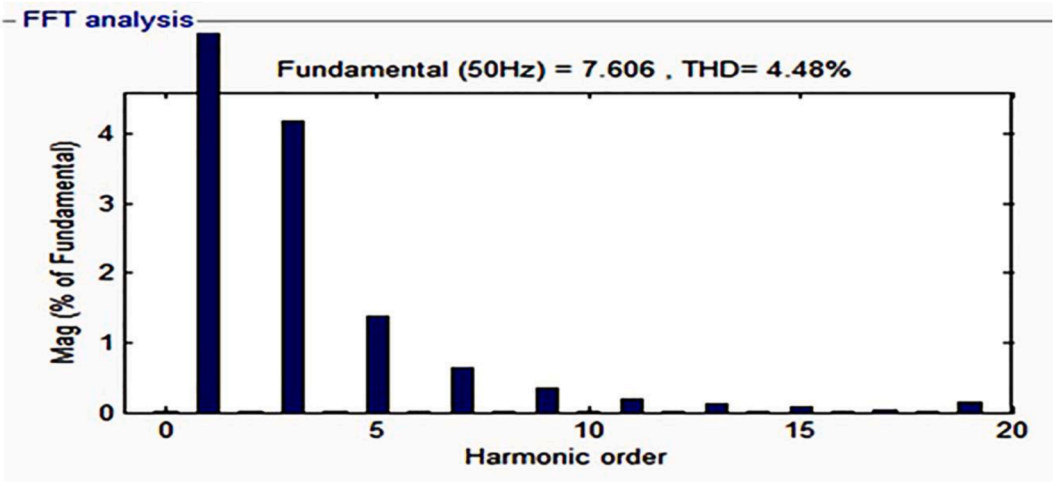

Fig. 37. Harmonic spectrum of input current with Boost converter.

and current, which contributes to effective power utilization. The system achieves a near-unity power factor of 0.996, reflecting excellent efficiency in power transfer and reduced reactive power. The harmonic distortion is maintained at 4.48 %, ensuring compliance with quality standards and minimal impact on the power system.

7. Hardware implementation

The laboratory model of 100 W Cyclo-inverter IH System was made to check the simulation results. Simulation results of Cyclo-inverter fed from AVC-PWM control techniques is verified by the practical results. Hardware test setup of suggested system is shown in Fig. 38. The uncontrolled rectifier is built by 4 number of IN4001 diodes to supply DC voltage to the Cyclo-Inverter System. Subsequently it is formed by four IRF840 MOSFETs for changing DC into high frequency AC. The logic circuit is constructed by using a FPGA-SPARTAN 3E family-XC3s100E, TQ144 package controller, which provides gating signals to MOSFETs.

The gating signals are then amplified by using IR2110 driver which is used to provide isolation between low power and high power circuits. The induction heating load was made by a working coil consisting of 70 mm outer diameter and 4 mm thickness and the dimension of work piece is (300 × 300) mm. The values of the coil and the work piece are selected as per the simulation parameters. The current waveforms are measured by using an Agilent N2862B passive probe. All the output waveforms are measured and recorded by using KEYSIGHT Infiniti Vision DSO-X2002A type digital oscilloscope.

The driving pulses generated based on an AVC-PWM technique for various MOSFET are represented in Figs. 39, 40 and 41 respectively. The amplitude of each pulse is 3V. The first leg devices Q_1 and Q_2 with 40 % duty, devices in II leg Q_3 and Q_4 with 20 % duty and devices in common leg Q_5 and Q_6 are given with 50 % duty respectively. The voltage across load 1 and 2 are shown in Figs. 42 and 43. The current through load 1 and 2 are shown in Figs. 44 and 45. The peak value of voltage is 42 V and current is 4.4A respectively. Pulse Width Modulated system gives better performance in terms of efficiency and switching losses than Pulse Density Modulation (PDM) for low to medium power applications. The experimental waveforms from DSO henceforth prove that acoustic noise; losses during switching and settling time are minimized.

Table 4 shows that output voltage and currents obtained in hardware is somewhat less than its simulation outputs and also it is identified that a cyclo-inverter fed IH system gives best results in terms of output voltage and current.

8. Conclusion

The main objective is to search out the appropriate control procedure for obtaining greatest performance in two-output Cyclo-inverter topology. This is achieved by considering two different control techniques

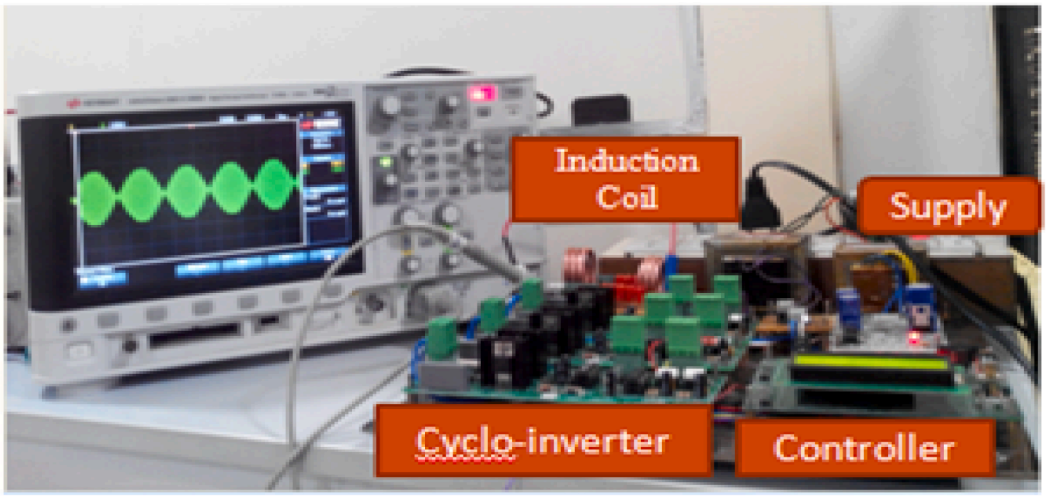

Fig. 38. Experimental Setup for Cycloinverter fed IH system.

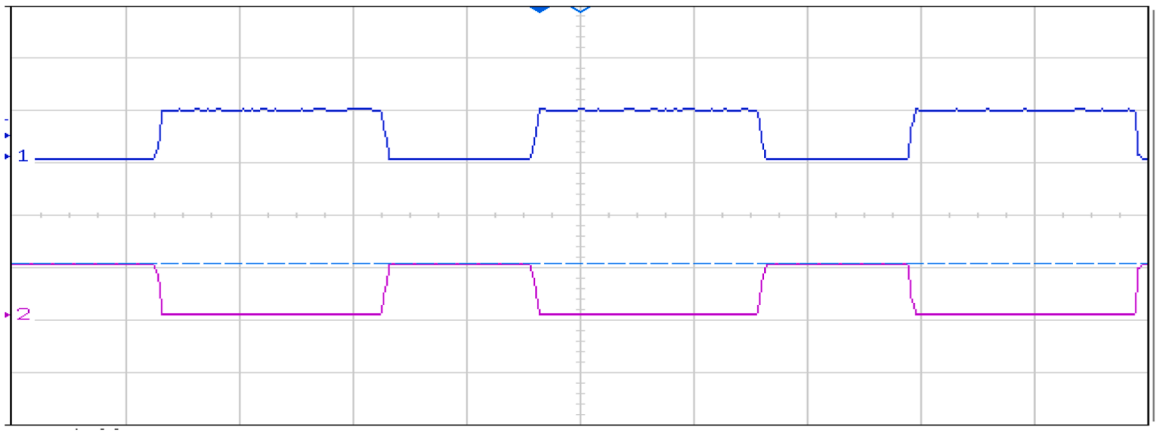

Fig. 39. Driving pulses of switches Q_1 & Q_2 (X-axis:9.5μs, Y-axis: 3V/div).

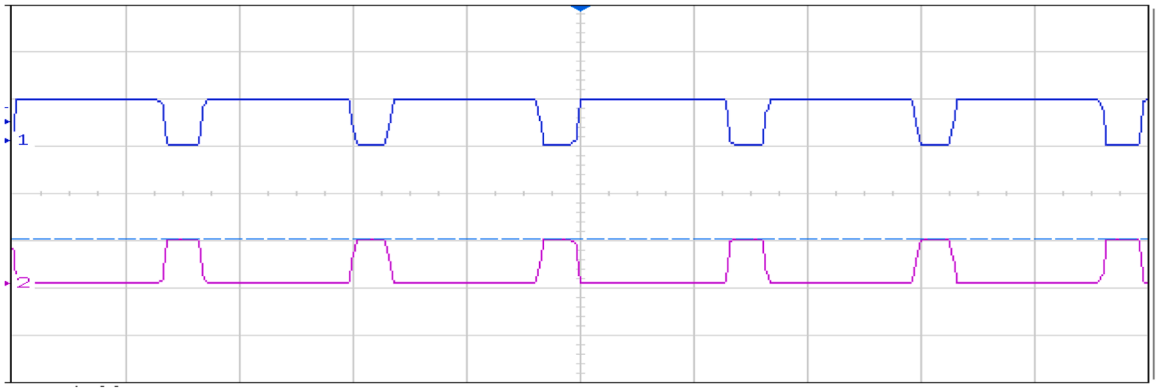

Fig. 40. Driving pulses of switches Q_3 & Q_4 (X-axis:9.5μs, Y-axis: 3V/div).

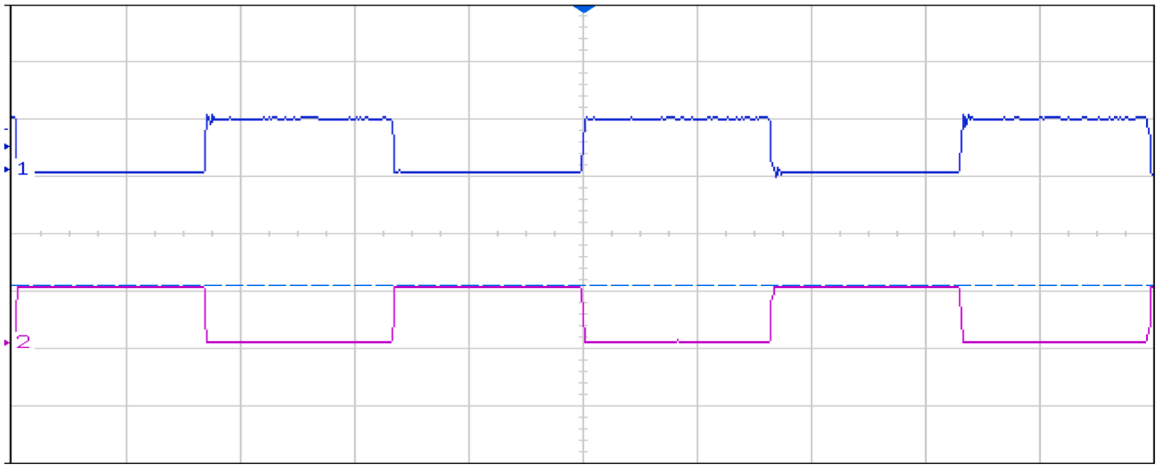

Fig. 41. Driving pulses of switches Q_5 & Q_6 (X-axis:9.5μs, Y-axis: 3V/div).

namely AVC-PDM and AVC-PWM techniques. The results of both techniques were presented and AVC-PWM is found to be the best one for obtaining greater power efficiency, energy efficiency with minimum THD value. In AVC-PDM control, P_{out} can be controlled by varying the angle alpha (phase delay), flickering effect is absent and wide range of soft switching is possible with variable load. The overall performance of a two-output cycloinverter-fed induction heating system depends heavily on tuning parameters like the duty cycle, load resistance, and switching frequency. Increasing the duty cycle boosts the output power, while higher load resistance reduces it. Furthermore, tuning the load to a specific switching frequency (30 kHz in this case) ensures maximum power transfer and efficiency. Deviating from this frequency causes the system to operate less efficiently, leading to reduced output power. The transient response parameters highlight the efficiency and precision of FL controllers in managing the dynamic behavior of the IH system, ensuring fast response and accurate steady-state performance.

Simulation of Cyclo-inverter fed IH system is also applicable for multiple power settings for a specified power rating. For different output levels on load side PI or PID Controller needs gain adjustment while FLC is adaptive for multiple power settings. And the proposed THD filter

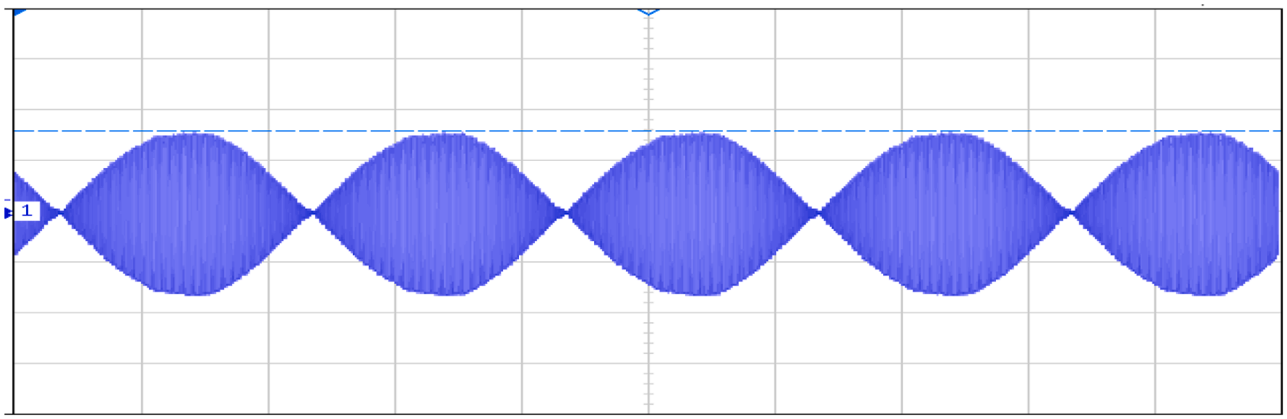

Fig. 42. Voltage across Load 1 (X-axis:8.3 μs, Y-axis: 20V/div).

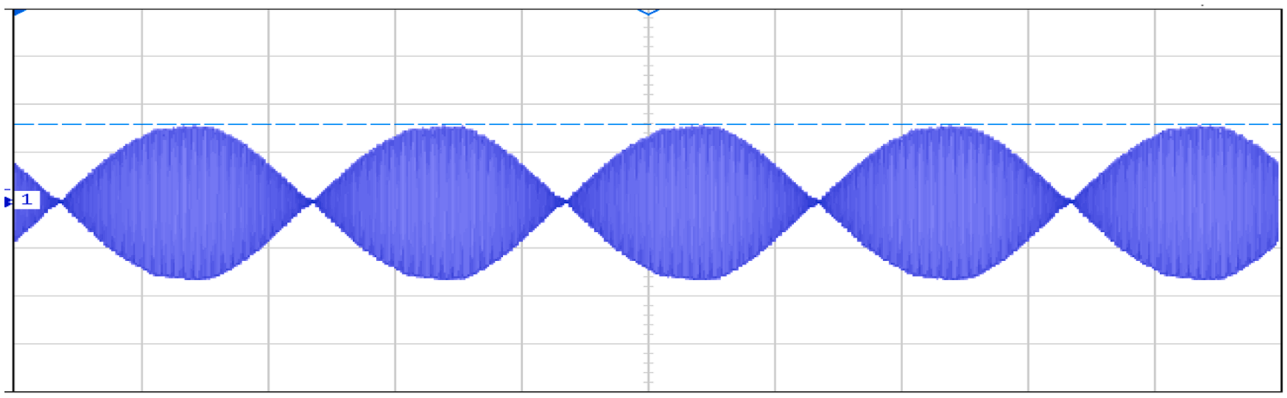

Fig. 43. Voltage across Load 2(X-axis:7.8 μs, Y-axis: 20V/div).

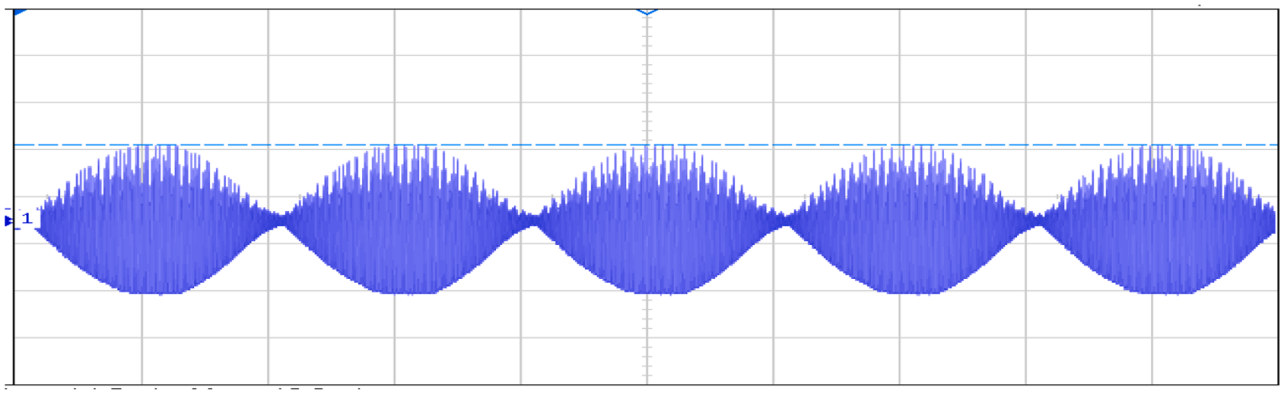

Fig. 44. Current through load 1(X-axis:8.3 μs, Y-axis: 2.5A/div).

underscore the effectiveness of the boost converter in enhancing power factor and maintaining power quality in the IH system. Hardware of Cyclo-Inverter fed IH System is fabricated & tested to validate the simulated waveforms. The experimental waveforms from DSO henceforth prove that acoustic noise losses during switching and settling time are minimized.

Induction heating system can be operated to give better power control strategy at higher switching frequencies. The comparison between hysteresis and Fuzzy controlled systems will be done in near future.

CRediT authorship contribution statement

S. Jaanaa Rubavathy: Writing – review & editing, Writing – original draft, Software, Methodology, Conceptualization. **Sivapriya J:** Investigation, Formal analysis, Data curation. **B. Durai Babu:** Resources, Project administration, Methodology. **K. Sasikala:** Writing – original draft, Supervision, Software. **S Gomathi:** Writing – review & editing, Visualization, Validation.

Declaration of competing interest

The authors declare that they have no known competing financial

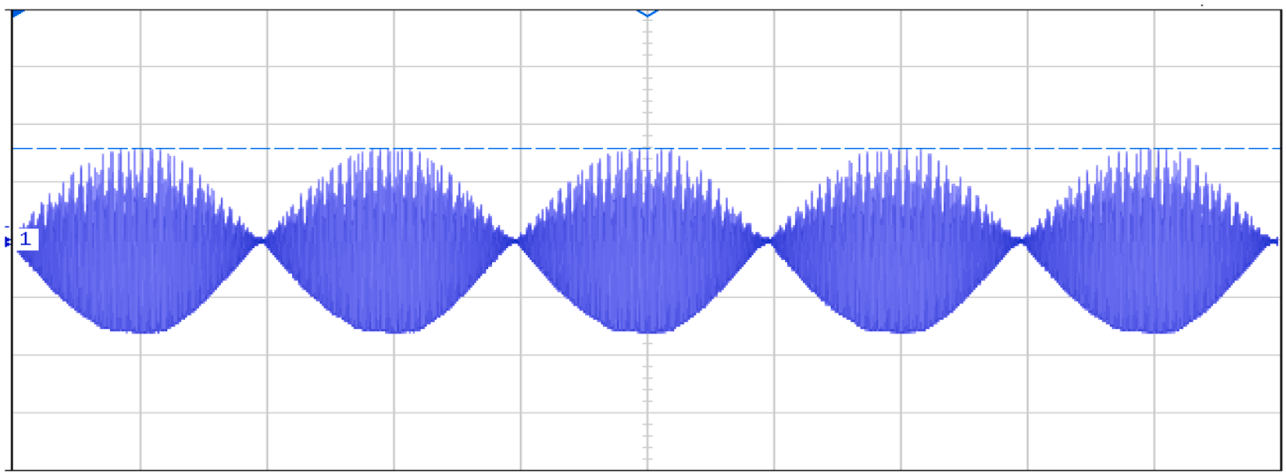

Fig. 45. Current through load 2(X-axis:7.8 μs, Y-axis: 2.5A/div).

Table 4
Comparison of simulation & hardware results.

	Simulation Results			Hardware Results		
	V_{in} (V)	V_0 (V)	I_0 (A)	V_{in} (V)	V_0 (V)	I_0 (A)
AVC-PWM based Cyclo-inverter fed IH	48	44	5.2	48	42	4.4

interests or personal relationships that could have appeared to influence the work reported in this paper.

Data availability

Data will be made available on request.

References

[1] M. Saravanan, A.Ramesh Babu, High power density multi-MOSFET-based series resonant inverter for induction heating applications, Int. J. Power Electron. Drive Syst.(IJPEDS) 7 (1) (March 2016) 107–113.

[2] Booma Nagarajan, Rama Reddy Sathi, Pradeep Vishnuram, Power tracking control of domestic induction heating using pulse density modulation with the Fuzzy logic controller, J. Electr. Eng. Technol. 9 (6) (2014) 1978–1987.

[3] H. Pham, H. Fujita, K. Ozaki, N. Uchida, Phase angle control of high frequency resonant currents in a multiple inverter system for zone-control induction heating, IEEe Trans. Power. Electron. 26 (11) (2011) 3357–3366.

[4] C. Carretero, O. Lucia, J. Acero, M. Burdio, Phase-shift control of dual half-bridge inverter feeding coupled loads for induction heating purposes, Electron. Lett. 47 (11) (May 2011) 670–671.

[5] Hirotaka Koizumi, Kosuke Kurokawa, Shinsaku Mori, Analysis of class D inverter with irregular driving patterns, IEEE Trans. Circuits Syst.-I 53 (3) (2006) 677–687.

[6] Rubavathy.S Jaanaa, P. Murugesan, Experimental investications on multi-output Cyclo-inverter fed induction heater system, Aust. J. Electr. Electron. Eng. (AJEEE) 10 (4) (2013) 483–489, 2013.

[7] Rubavathy.S Jaanaa, P. Murugesan, Simulation and verification of a multi output series resonant inverter fed induction heater system, in: IEEE International Conference on Power Electronics, Drives and Energy Systems (PEDES), Bengaluru, India, 2012. December 16-19.

[8] Rubavathy.S Jaanaa, P. Murugesan, Performance analysis on cyclo-inverter fed induction heating system with different control techniques, J. Comput. Theor. Nano Sci. 14 (3) (2017) 1–8.

[9] Jesus Acero, Claudio Carretero, Rafael Alonso, Jose M. Burdio, Quantitative evaluation of induction efficiency in domestic induction heating applications, IEEE Trans. Magn. 49 (4) (April 2013) 1382–1389.

[10] Hector Sarnago, Oscar Lucia, Arturo Mediano, Jose M. Burdio, Direct AC-AC resonant boost converter for efficient domestic induction heating applications, IEEe Trans. Power. Electron. 29 (3) (March 2014) 1128–1139.

[11] Comparison on current source rectifier and inverter topologies of induction heating power supply for forging applications, in: The 20th International Conference on Electrical Machines and systems, Sydney, NSW, Australia, ICEMS, 2017, pp. 1–6. August 11-14.

[12] Feiyan Li, Jin Wang, Jingang Li, Ke Li, Analysis of LLC dual-frequency induction heating power supply with time sharing control, in: The 13th IEEE conference on Industrial Electronics and Applications (ICIEA), Wuhan, China, 2018, 31 May to 2 June 2018.

[13] Kumaraswamy.A Ananyo Bhattacharya, Pradip Kumar Sadhu, Dual output and dual frequency resonant inverter based induction heating using ADC control, IETE J. Res. 70 (3) (2024) 3087–3099.

[14] Wei Han, Kwok Tong Chau, Hoi Chun Wong, Chaoqiang Jiang, Wong Hing Lam, Article all-in-one induction heating using dual magnetic couplings, Energies (2019) 1–17, 201912, 1772.

[15] Pattanapong Kongsakorn, Anuwat Jangwanitlert, A two-output High frequency series- resonant induction heater, in: IEEE International Conference on Electrical Engg /Electronic, Computer, Telecommunications & Information Technology, 2010, pp. 842–845.

[16] Pradeep Vishnuram, R. Sridhar, A hybrid AVC and PDM aided full bridge resonant converter for induction heating application, ISSN: 2277-3878, Volume-7 Issue-6S6, Int. J. Recent Technol. Eng. (IJRTE) (April 2019). ISSN: 2277-3878, Volume-7 Issue-6S6.

[17] Nagarajan Booma, Rama Reddy Sathi, Pradeep Vishnuram, "Comparative analysis of various modulation strategies for induction heating system" Appl. Mech. Mater., 10.4028/www.scientific.net/AMM.622.39.

[18] Senthil Rajan Ramalingam, C.S. Boopathi, Sridhar Ramasamy, Mominul Ahsan, Julfikar Haider, Mohammad Shahjalal, A single-coil multi-tapped PDM-based induction heating system for domestic applications, Electronics 12 (2023) 404, https://doi.org/10.3390/electronics12020404.

[19] P.Ramachandiran Vishnuram, G. Sudhakar Babu, T. Nastasi, B. Induction heating in domestic cooking and industrial melting applications: a systematic review on modelling, converter topologies and control schemes, Energies 14 (2021) 6634, https://doi.org/10.3390/en14206634.

[20] S.H. Hosseini, A.Y. Goharrizi, E. Karimi, A Multi-Output series resonant inverter with asymmetrical voltage-cancellation control for induction-heating cooking appliances, in: 2006 CES/IEEE 5th International Power Electronics and Motion Control Conference, Shanghai, China, 2006, pp. 1–6, https://doi.org/10.1109/IPEMC.2006.4778290.

[21] Eram Bushra, Kamran Zeb, Iftikhar Ahmad, Muhammad Khalid, A comprehensive review on recent trends and future prospects of PWM techniques for harmonic suppression in renewable energies based power converters, Results. Eng. 22 (2024), https://doi.org/10.1016/j.rineng.2024.102213.

[22] Pradeep Vishnuram, Gunabalan Ramachandiran, Sridhar Ramasamy, Suchitra Dayalan, A comprehensive overview of power converter topologies for induction heating applications, Int. Trans. Electr. Energ. Syst. 30 (2020) e12554, https://doi.org/10.1002/2050-7038.

[23] A. Kumar, A. Goswami, P.K. Sadhu, J.R. Szymanski, Single-stage LLC resonant converter for induction heating system with improved power quality, Electricity 5 (2024) 211–226, https://doi.org/10.3390/electricity5020011.

[24] Jaanaa Rubavathy S, D. Sungeetha, M.J. Carmel Mary Belinda, Jayant Giri, Emad Makki, Hitesh Panchal, P. Deepa, S. Gomathi, J. Aravind Kumar, T. R. Praveenkumar, An inimitable Elman network based fire hawk controller and skill optimized power tracker with ultra gain converter for improving the performance of PV tied EV systems, Case Stud. Therm. Eng. (2024), https://doi.org/10.1016/j.csite.2024.104183.

[25] S. salehi, K. Abbaszadeh, S.G. Sani, H.Haji Mohamadi, A new domestic induction heating resonant converter with high power conversion efficiency, in: 2021 12th Power Electronics, Drive Systems, and Technologies Conference (PEDSTC), Tabriz, Iran, 2021, pp. 1–6, https://doi.org/10.1109/PEDSTC52094.2021.9405878.

[26] Armando Rojas-Morín, Yolanda Flores-Salgado, Omar Alvarez, Alejandro Jaramillo-Mora Brito, Arturo Barba-Pingarrón, Thermal analysis using induction

and concentrated solar radiation for the heating of metals, Results Eng. 14 (2022) 1–12, https://doi.org/10.1016/j.rineng.2022.100431.

[27] Sushanta Roy, Syed Ishtiaq Ahmad, Md.Shafiqur Rahman, Mohammed Salauddin, Experimental investigation on the influence of induction furnace slag on the fundamental and durability properties of virgin and recycled brick aggregate concrete, Results Eng. 17 (2023), https://doi.org/10.1016/j.rineng.2022.100832.

[28] M. Badaruddin, S.Sumardi Sugiyanto, D. Asmi, Improvement of the fatigue crack growth resistance in AISI 4140 steel under single- and multi-austempering heat treatments, Results Eng. 21 (2024), https://doi.org/10.1016/j.rineng.2024.101814.